Atmospheric Stability Intervals Influencing the Potential for Off-Target Movement of Spray in Aerial Application

Steven J. Thomson[1], Yanbo Huang[*2], and Bradley K. Fritz[3]

[1]United States Department of Agriculture, National Institute of Food and Agriculture, Division of Agricultural Systems, Washington D.C., USA

[2]United States Department of Agriculture, Agricultural Research Service, Crop Production Systems Research Unit, Stoneville, MS, USA

[3]Bradley K. Fritz, United States Department of Agriculture, Agricultural Research Service, Aerial Application Technology Research Unit, College Station, TX, USA

*yanbo.huang@ars.usda.gov; 662-686-5354.

Abstract

A tower was equipped with temperature and wind-speed sensors at different heights to monitor weather conditions needed to quantify atmospheric stability throughout the day. Data presented in this study showed consistent patterns of atmospheric stability occurring primarily between the hours of 18:00 and 06:00 hrs during summer months on clear days. Further, our results verified correctness of the three-degree rule in Arkansas when spraying on clear days in the summer months. This study is informative for pilots and farm managers to schedule aerial application assuring that spraying will not occur under stable atmospheric conditions to avoid off-target drift.

Keywords

Aerial Application; Spray Drift; Temperature Inversion; Atmospheric Stability; Stability Ratio; Crop Protection

Introduction

Crop protection materials and harvesting aids applied from both aircraft and ground sprayers can drift off-target due to many factors such as nozzle type and orientation, spray pressure, and application height. Droplet size, which is influenced by nozzle and spray formulation interaction, is a significant factor for near-field off-target drift (Ozkan, 1998). Uncontrollable weather factors must also be considered, and it is incumbent on the applicator to schedule application during periods that do not exacerbate off-target drift or off-target movement of spray. For good environmental stewardship from aerial application of crop protection materials, it is essential that the applicator avoid application under 'stable' atmospheric conditions when a temperature inversion is likely to occur. Spraying must not occur where a temperature inversion prevents the spray cloud settling within the treated area (FAO, 2001). The detrimental effects on cotton of spraying 2, 4-D to rice or pastures under conditions of a temperature inversion have been documented (Bennett, 2006). Based on field and extension reports the increased number of drift complaints in East Arkansas were most likely the result of multiple applications of 2,4-D under stable atmospheric conditions. Under those conditions, a parcel of air cannot rise and disperse, but it can move laterally in the light variable winds typical of a surface inversion (Ramsey, 2001). The plumes of small droplets remaining suspended in air is dispersed through the atmospheric boundary layer in much the same manner as other air pollutants (Stoughton et al., 1997). A spray layer applied under stable conditions is thus "ready to move" off target when the wind picks up (Bennett, 2006). Basic studies have been performed to quantify the mechanisms and to model increase in wind speed due to morning heating of the atmospheric boundary layer (Lapworth, 2006). Although not indicated as an example application, these relationships also have a direct effect on when it is safe to spray crop protection materials. Mahrt et al. (1998) attempted to characterize weakly stable, transition-stable, and very stable nocturnal boundary layer regimes in a heavily instrumented set of experiments as a function of several

2327-7246/17/01 001-6 © 2017 DEStech Publications, Inc.
doi:10.12783/ijast.2017.0501.01

factors including wind. Although aerial spraying does not typically occur at night, these relationships could be useful in examining spray cloud movement from nocturnal ground spraying. Miller and Stoughton (1999) actually tracked plumes of small droplets as a function of atmospheric stability. As expected, the time that it took for droplet dispersal was primarily controlled by atmospheric stability.

Surface temperature inversions occur during night-time surface cooling and until morning surface heating (Beychock, 1994; Ramsey, 2001). These conditions usually occur at sunset to just after sunrise, under windless to low wind conditions, and under clear to partly cloudy skies. Other indicators are the presence of ground fog (if sufficient humidity exists), dust hanging over a roadway, smoke from a chimney forming a layer, and dew or frost (also if sufficient humidity exists). However, many of these indicators illustrate the 'potential' for temperature inversions and duration of these events can be highly variable. For the latitude of College Station, TX, Fritz et al. (2008) indicated that stable atmospheric conditions (unfavorable for spraying) occurred when wind speeds were 2.0 m s-1 or below. The authors also documented that daytime (06:00 to 18:30) temperature inversions occurred between 57 and 65% of the monitored days.

Some States in the US where aerial application is prevalent have adopted guidelines for management of spray drift from ground and aerial applications, but recommendations vary widely and in scope regarding spray application under conditions favorable for temperature inversion or stable atmosphere. Section 219.06 of Mississippi applicators licensing rule (MDAC, 2016) states "Smoke and/or other suitable means shall be used to detect inversion conditions and determine wind direction and speed." This refers to the direction of smoke as an indicator of whether it is safe to spray. A guideline from Australia (CSIRO, 2002) indicates that the presence of an inversion can also be indicated by driving a vehicle along a dusty track and observing movement of dust, and the EPA has proposed a pesticide applicators rule that requires applicators show proficiency in use of smoke generators for determining off target movement of spray (Wiggins, 2015).

Because of concerns such as those outlined by Bennett (2006), guidelines in Arkansas have been revised to include quite specific language concerning conditions to avoid spraying during an atmospheric temperature inversion. A rule from the Arkansas State Plant Board (ASPB, 2008), states that "Herbicide applications may not be made under conditions where the spray may possibly be entrained in an inversion layer." The regulation goes on to state "As an indicator that an inversion is unlikely to exist, the applicator shall record the ambient temperature measured at the field of application for each application. Inversions are much less likely to exist if the temperature has increased three (3) degrees Fahrenheit from the morning low at the time of application for applications made before noon or has not decreased more than three (3) degrees Fahrenheit from the afternoon high for applications made after noon." It is not clear however, where information to develop these guidelines originated, and no seasonal dependency was implied for the recommendation. It would thus be useful and instructive to document the time and duration of stable atmosphere and temperature profiles on a seasonal basis to present better guidelines for agricultural pilots. By using an instrumented tall tower, temperature and wind profiles that indicate both the presence of surface and aloft temperature inversions and ultimately, atmospheric stability known to influence off-target movement of spray, could be determined. This study presents data from towers used to calculate stability ratios. These data can help facilitate recommendations on times of day that are likely to be of concern when spraying crop protection materials.

Objectives

Objectives of this study were

1.To measure weather variables on an instrumented tower and use these data to determine temporal atmospheric stability.

2.To use atmospheric stability criteria from example periods representing a range of conditions to determine times of day and weather conditions favorable for a stable atmosphere.

3.Using stability criteria, develop guidelines for aerial applicators on times of day, wind conditions, air

temperatures, and times of year to avoid spraying under stable atmospheric conditions

Materials and Methods

A tall tower was set up at the USDA ARS CPSRU Mechanization Research Farms, Stoneville, MS (Figure 1). The tower was equipped with Omega 44000 series precision thermistors of 0.1% interchangeability to measure air temperatures, Qualimetrics model 2030 anemometers to measure wind speed, and a Met-One 024A wind direction sensor. The temperature sensors were placed at 4.6, 9, 14, 18.3, 23, and 27.4 m for temperature; 4.6, 12, 20, and 27.4 m for monitoring wind speeds.

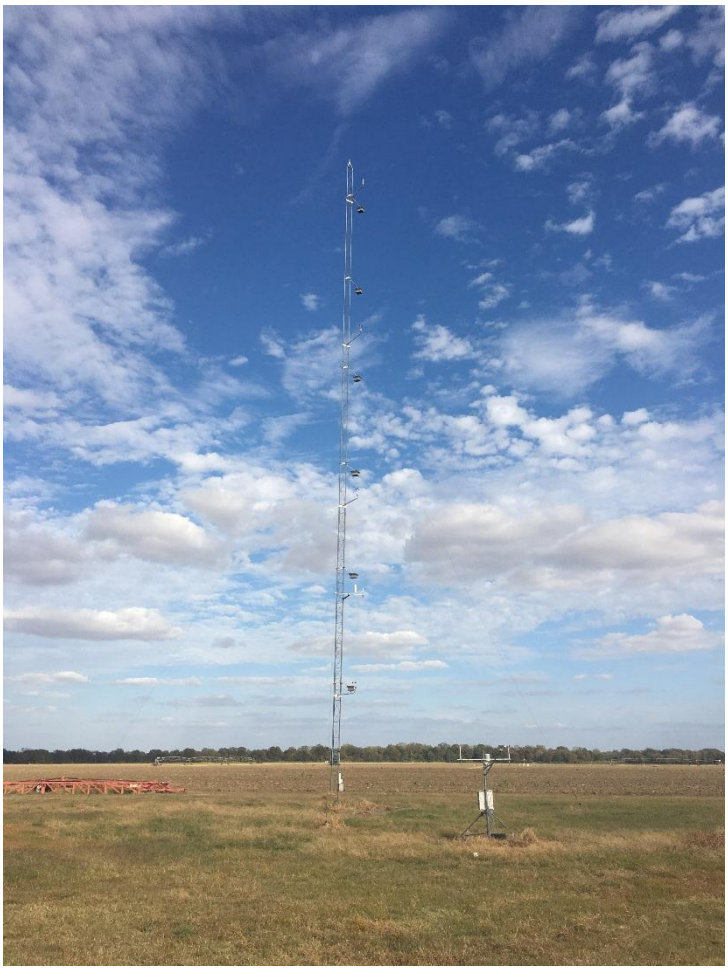

FIGURE 1. TALL WEATHER TOWER FOR DATA ACQUISITION.

A Campbell CR-21X micrologger was used for data acquisition and was setup in pulse counting mode for the wind speed sensors. The CR-21X was programmed in a half-bridge mode with precision completion resistors to measure output from the thermistors using 5000 mv excitation. The wind direction sensor also utilized the precise excitation voltage. Weather data were obtained from April through October 2004 and read every five minutes. These data were periodically downloaded from data cans for further processing using a custom-designed program written in SAS 8.2 (SAS Institute, Cary, NC, USA). This program created a spreadsheet file from raw data for each block of downloaded data, and data files for each month were created. Data read every five minutes were averaged over a one hour period and a resulting spreadsheet file was regenerated using a custom routine programmed in Matlab® R2010a (Mathworks, Natick, MS USA).

Using the collected meteorological data, the Stability Ratio (SR) (Munn, 1966) was calculated as:

$$SR = \frac{T_{z_2} - T_{z_1}}{WS_{z_3}^2} \cdot 10^5 \quad (1)$$

where T_{Z_1} and T_{Z_2} are temperature (oC) at height z1 and z2 and WS_{Z_3} the wind speed (cm/sec) measured at a height of z3 between z1 and z2,, which is the measured equidistant between z1 and z2 on a log scale. Yates et al. (1974) used heights of 2.4 and 9.8 m for z1 and z2, respectively, and a wind speed measurement height of 4.9 m.

To calculate SR, temperatures were measured at 4.6 m and 9 m for T_{Z_1} and T_{Z_2}. Wind speed WS_{Z_3} was measured at 4.6 m. This height was not equidistant between the two temperature levels for strict application of Equation (1), but this discrepancy will be addressed later. Diurnal atmospheric stability can be determined based atmospheric stability classes as illustrated Table 1 for calculation of stability ratio.

TABLE 1. ATMOSPHERIC STABILITY CATEGORIES AS A FUNCTION OF STABILITY RATIO (SR) RANGES (YATES ET AL., 1974)

Atmospheric Stability Category	SR Range
Unstable	-1.7 to -0.1
Neutral	-0.1 to 0.1
Stable	0.1 to 1.2
Very Stable	1.2 to 4.9

Results and Discussion

Before evaluating ASPB (2008) criteria for daytime spraying at transition times between stable and unstable states, it is instructive to determine the likelihood that safe spraying could occur during night-time hours. Night spraying is sometimes desirable for ground spraying, although aerial spraying at night is primarily conducted in the Southwest U.S. deserts, far from neighboring areas. Data presented in the study presented herein showed consistent patterns of atmospheric stability primarily between the hours of 1800 and 0600 in the summer months, which is also consistent with a study in College Station, TX (Fritz et al., 2008). Figure 1 illustrates a 63% average probability of either stable or strongly stable conditions occurring between 1900 and 0600 over the period of 14 April 2004 to 6 November 2004. Neutral conditions occurred 23% of the time and unstable conditions occurred 14% of the time. Probability of either stable or strongly stable conditions over the logging period was 63%, which compares well with 57 % and 65% of days monitored in Texas over two different stations. Enough wind at night can cause sufficient mixing and create unstable atmospheric conditions suitable for spraying. It is cautioned, however, that ground spraying during high winds can exacerbate off–target near-field drift.

Figures 3 through 7 illustrate weather data and stability ratios representing a range of atmospheric combinations over a single season. As Equation (1) is mechanistic and simply requires combinations of wind and temperature values to determine atmospheric stability, five days over the cropping season were chosen to illustrate a range of conditions that would be encountered by aerial applicators to make decisions on whether to spray based on results obtained from Equation (1). Diurnal changes that influence atmospheric stability were clearly illustrated within these periods. Table 2 shows transitional periods and stability ratios for the five selected dates. For 15 April 2004 (Figure 2), the transition point from stable conditions (unfavorable for aerial application) to unstable conditions in the morning hours occurred between about 06:00 and 07:00. This response characterizes a typically smooth transition between states as categorized in Table 1. It is interesting to note that stable or very stable conditions were still prevalent at relatively high wind speeds (between 1.25 to 1.60 m s-1). In the evening, stable conditions began to occur after about 18:00 (6:00 PM) at very low wind speed (0.23 m s-1) and 4.6 m height.

The plot of 15 July (Figure 2) indicates more variable wind, although diurnal temperature cycles followed a similar smooth pattern as did the 15 April plot. Within the morning hours normally indicating stable conditions, fluctuations between stable and unstable conditions inversely tracked wind speed fluctuations, as would be expected. Evening hours showed transition to stable conditions after 18:00 as in the 15 April plot, and stable conditions were clearly in place when wind speed decreased to 0.67 m s-1. The 16 August plot (Figure 5) shows a similar trend to the July plot except that the 'strength' of late afternoon stability at 19:00 was not as great. Wind speed was higher (1.52 m s-1) as compared with 1.51 m s-1 in July. The atmosphere was still classified as 'stable' at

a wind speed of 1.52 m s-1 on 16 August.

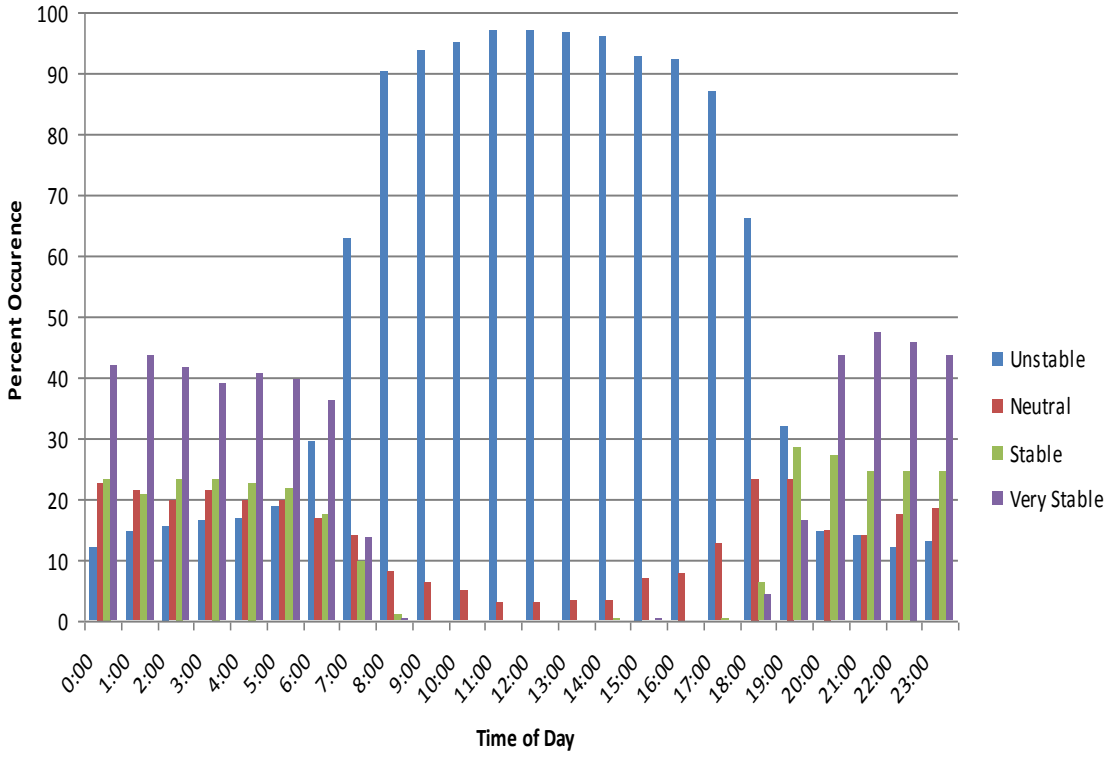

FIGURE 2. PROBABILITY DISTRIBUTION OF ATMOSPHERIC STABILITY CLASSIFICATION BY TIME OF THE DAY BETWEEN 14 APRIL, 2004 AND 6 NOVEMBER, 2004.

Not until 08:00 were neutral conditions established (Table 2) for either 15 September or 15 October (Figures 6 and 7, respectively). Figure 7 illustrates weakly stable conditions during the early morning hours after midnight because of higher wind speeds hovering in the 1.11 m s-1 range until 08:00. The transition to stable conditions in the evening occurred after 1800 as the wind speed measured at 4.6 m dipped to 0.89 ms-1. The 15 September plot indicated high winds continuing until midnight and corresponding neutral conditions. Stable conditions became apparent as the wind speed slowed at night.

Table 2 indicates that the criteria for unstable or neutral conditions suitable for spraying were satisfied at 07:00 on both 15 July and 16 August. Criteria for neutral or unstable conditions were not satisfied until 08:00 in April, September, or October. As indicated herein, a rule written for Arkansas (ASPB, 2008) indicates a required 1.67 º C temperature rise in the morning hours before aerial spraying can occur safely (in neutral or unstable atmosphere). Temperature rise as specified by the ASPB rule to achieve these conditions was exceeded on all example days except 15 April. This could be a significant finding as aerial spraying for burn-down herbicide customarily occurs in the late winter and early spring, so pilots may thus need to delay spraying in the morning during the cooler months. Stable or very stable conditions returned by 1900 in July and August and by 18:00 in April and October. The values for September are not shown because higher winds kept conditions unstable during this period (Figure 6). The ASPB rule of stopping spray before a 1.67 º C temperature decrease appeared to be exceeded for all example dates shown in Table 2 except April. However, an unstable condition was still indicated on 15 July when this value was exceeded indicating that a 1.67 º C reduction was rather conservative. Likewise, the temperature reduction result almost matched a 1.67 º C for 15 August while unstable conditions still prevailed. For July and August however, the ratio indicating instability was rather weak (-0.40 and -0.41 respectively) at 18:00. In April, wind was very calm in the afternoon and atmosphere became very stable rapidly before air temperature measured at 4.6 m decreased appreciably. The transition from stable to very stable conditions thus indicated high sensitivity to small temperature inversions after 17:00.

TABLE 2. ATMOSPHERIC STABILITY RATIOS FOR FIVE SELECTED DATES USING AIR TEMPERATURES MEASURED AT 4.6M AND 9.8M. TEMPERATURE CHANGE INDICATED IN BOLD DUE TO CHANGE OF STATE CAN BE COMPARED WITH GUIDELINES FOR REQUIRED 1.67 º C TEMPERATURE DIFFERENCE (INCREASE IN MORNING; DECREASE AT NIGHT) TO ASSURE UNSTABLE CONDITIONS (ASPB, 2008).

Julian Day	Date	Time	Time offset from sunrise/sunset (min)	Stability Classification	Stability Ratio	Wind Speed (m/s)	Air Temperature (º C), 4.6m	Temperature Change (º C)	ASPB Criteria Met?
106	15-Apr	06:00	-33	V-stable	3.67	1.23	9.50	0.40	
		07:00	27	Stable	0.76	1.64	11.20	2.10	
		08:00	87	Neutral	-0.08	2.73	13.70	**4.60**	Yes
		17:00	-155	Unstable	-1.70	0.23	24.20	-0.05	
		18:00	-95	V-stable	4.90	0.23	23.30	**-0.92**	No
197	15-Jul	06:00	-5	V-stable	4.90	0.39	24.70	0.33	
		07:00	55	Unstable	-0.39	1.13	27.00	**2.69**	Yes
		18:00	-134	Unstable	-0.40	1.98	34.00	-1.94	
		19:00	-74	V-stable	4.90	0.67	31.60	**-4.34**	Yes
229	16-Aug	06:00	-27	V-stable	4.90	0.23	14.90	0.03	
		07:00	33	Unstable	-1.70	0.23	17.20	**2.30**	Yes
		08:00	93	Unstable	-1.70	1.22	22.00	7.14	
		18:00	-108	Unstable	-0.41	2.26	29.00	-1.62	
		19:00	-48	Stable	1.06	1.52	26.30	**-4.34**	Yes
259	15-Sep	07:00	13	V-stable	2.66	0.97	21.50	0.83	
		08:00	73	Neutral	-0.08	3.76	24.40	**3.51**	Yes
289	15-Oct	07:00	-8	Stable	0.63	1.93	7.82	0.44	
		08:00	52	Neutral	0.03	2.11	10.11	**2.72**	Yes
		17:00	-89	Neutral	-0.05	2.86	21.91	0.51	
		18:00	-29	Stable	0.99	1.29	19.49	**-2.66**	Yes

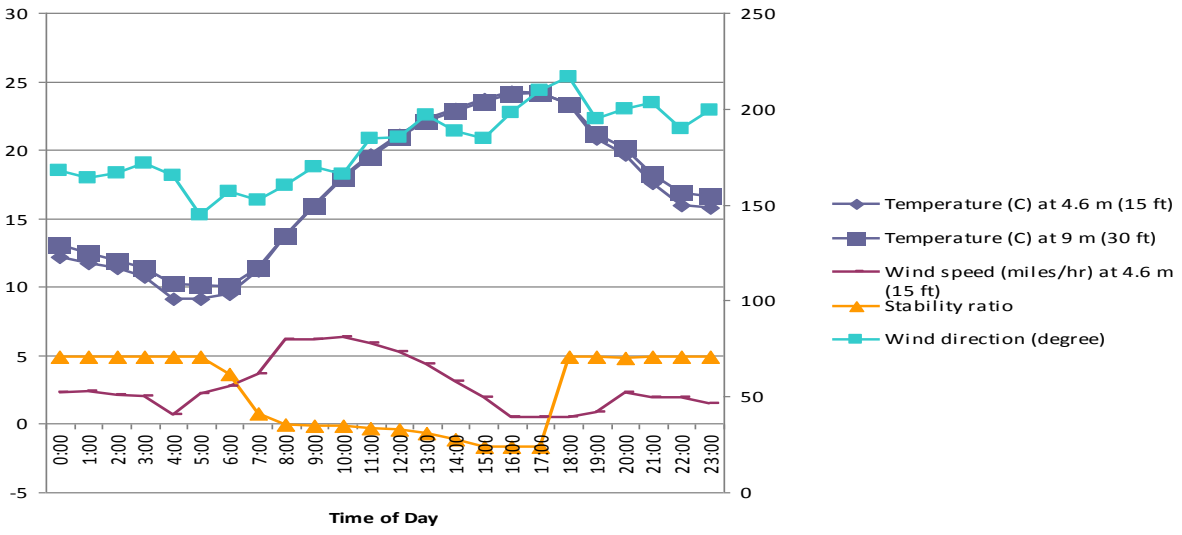

FIGURE 3. STABILITY RATIOS, TEMPERATURES, AND WIND FOR 15 APRIL, 2004. RIGHT AXIS IS THE SCALE FOR WIND DIRECTION (1 MILE/HR = 0.447 M/S).

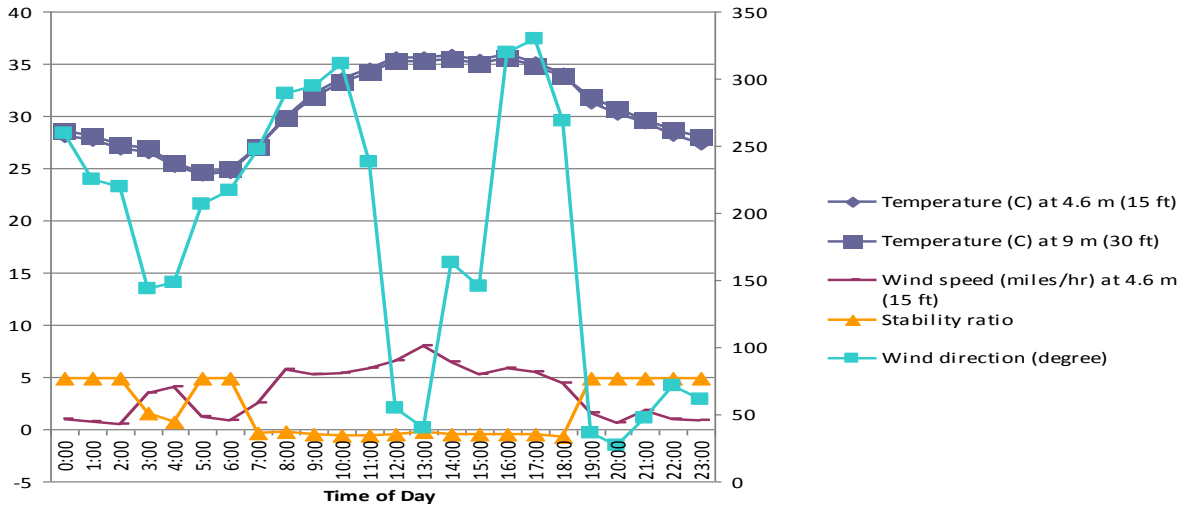

FIGURE 4. STABILITY RATIOS, TEMPERATURES, AND WIND FOR 15 JULY, 2004. RIGHT AXIS IS THE SCALE FOR WIND DIRECTION (1 MILE/HR = 0.447 M/S).

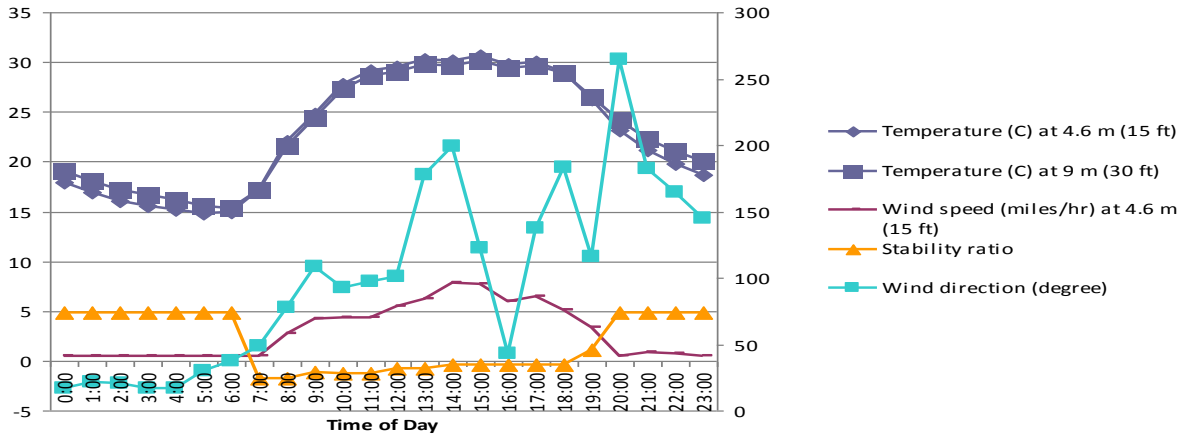

FIGURE 5. STABILITY RATIOS, TEMPERATURES, AND WIND FOR 16 AUGUST 2004. RIGHT AXIS IS THE SCALE FOR WIND DIRECTION (1 MILE/HR = 0.447 M/S).

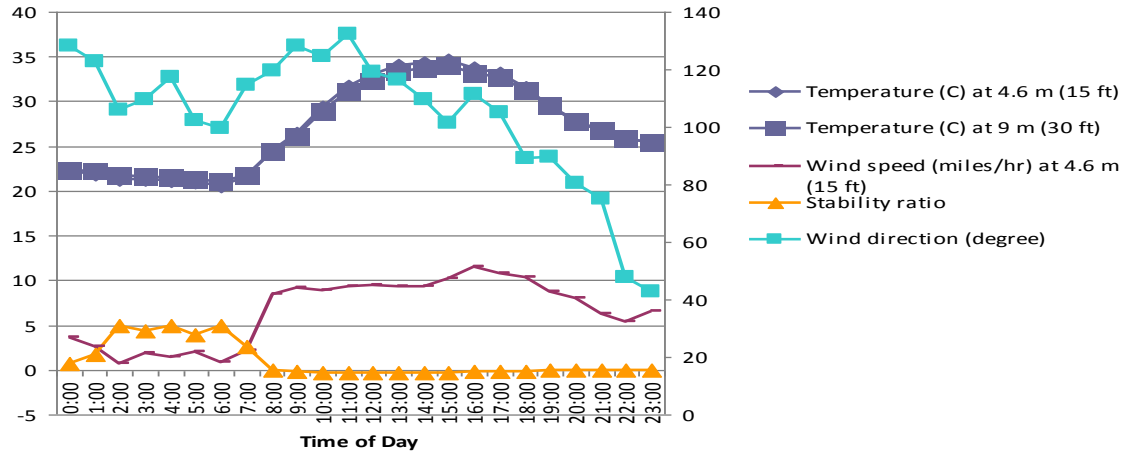

FIGURE 6. STABILITY RATIOS, TEMPERATURES, AND WIND FOR 15 SEPTEMBER, 2004. RIGHT AXIS IS THE SCALE FOR WIND DIRECTION (1 MILE/HR = 0.447 M/S).

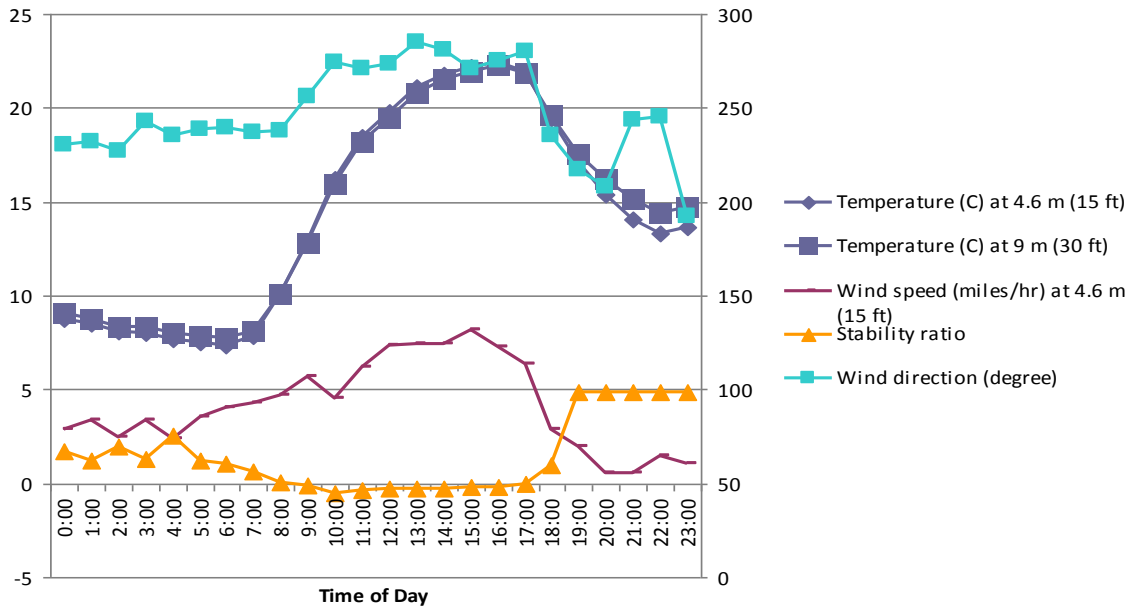

FIGURE 7. STABILITY RATIOS, TEMPERATURES, AND WIND FOR 15 OCTOBER, 2004. RIGHT AXIS IS THE SCALE FOR WIND DIRECTION (1 MILE/HR = 0.447 M/S).

Weather Considerations and Strict Application of the Stability Equation

There was somewhat of a discrepancy between wind speeds indicating stable atmosphere from Stoneville and College Station, TX. At the Stoneville location (and as discussed), wind speeds measured at the 4.6 m height in the morning typically ranged from 1.25 to 1.60 m s-1 during the transition from stable to unstable conditions (the former being unfavorable conditions for spraying). The College Station study indicated higher wind speed (2.0 ms-1), but this value was interpolated at 5.0 m based on wind speeds measured at 2.5 and 10 m heights. This was done to assure that Equation (1) would be used as intended (with wind speed measured at a height between the two temperatures). The equation used to interpolate that value (Fritz et al., 2008) is presented by Cooper and Alley (1994) as a logarithmic interpolation:

$$\frac{u_2}{u_1} = \left(\frac{z_2}{z_1}\right)^p \tag{2}$$

where

z_1, z_2 = elevations 1 and 2 (m)

u_1, u_2 = wind speeds at z_1 and z_2, m s^{-1}

p = exponent, unitless

To determine relative accuracy of this equation, data from the weather tower obtained at two heights and the interpolation equation (Equation (2)) were used to find wind speed at the intermediate height for comparison with measured values.

An example set of readings and calculations for two pairs are illustrated in Table 3. For each pair, the exponent p was determined and then used to calculate the wind speed at intermediate heights using wind speed at both the lower height (Z1) and the higher height (Z2). Results illustrate that results differed depending on which height was used in the log interpolation equation, but in no case did the interpolated value exceed the measured value by more than 6.3%. This indicates that the interpolated wind speed below which stable conditions unfavorable for spraying occurred (Fritz et al., 2008) at College Station TX (2.0 m s-1 vs. 1.25 - 1.60 m s-1 at Stoneville) was probably not too high an estimate for that location.

TABLE 3. WIND SPEEDS INTERPOLATED FROM TOWER DATA USING LOG FUNCTION (COOPER AND ALLEY, 1994). CALCULATED VALUES ARE IN BOLD.

U_1	1.2	2.0
U_2	2.5	3.4
Ratio of U	2.1	1.7
Z_1	4.6	12.2
Z_2	19.8	27.4
Ratio of Z	4.33	2.25
P	0.50	0.62
Interpolation of wind speed at intermediate height		
Desired height from which to obtain wind speed (m)	12.2	19.8
Actual (target) wind speed (m s^{-1})	2.02	2.56
Interpolated wind speed using wind speed at Z_1	**1.57**	**2.47**
Interpolated wind speed using wind speed at Z_2	**2.01**	**2.73**
% difference from actual wind speed (using Z_1)	28.7	3.5
% difference from actual wind speed (using Z_2)	0.5	-6.3

The study presented herein measured wind speed within 0.4 m of the specified height (4.6 m) but the air temperature at the lower height for application of Equation (1) was measured at the same height as wind speed. Strict application of Equation (1) requires that wind speed be measured between the two temperatures, so the interpolation procedure of Equation (2) could also be used here (Fritz et al., 2008). However, because temperature at the lower height was measured at 4.6 m instead of 2.4 m, stability factors would be calculated based on temperature combinations slightly above the atmospheric layer within which spraying occurs. So, we chose instead to extrapolate the temperature to 2.5 m based on temperature trends at other heights. This would allows strict application of Equation (1) within the correct layer (Yates et al., 1974), and data could be compared to determine if Equation (1) still gave acceptable results using data acquisition heights in our study.

To extrapolate temperature at the 2.5 m height, curve fits for air temperature vs. height were developed around transitions illustrated in Figs. 2 through 6 between unstable and stable conditions. Figures 8 through 12 illustrate trends in air temperature as a function of height, and the air temperature at the 2.5 m height could be obtained from the curve fit for each graph. We were careful to consider 'expected' trends when choosing a curve fit. Monotonic functions were used wherever possible, as these can also give accurate information on the inflection point (for example to find the height at which an inversion switches to non-inversion at a given time) as indicated by the first derivative. As an example, Figure 13 illustrates the first derivative of the Hoerl model used to fit temperature data at 0700 on 15 April (Figure 8 (a)) indicating a zero slope at 10.63 m height. A plot is also shown of the first derivative of a polynomial fit of the same data, which does not give an accurate result, consistent with issues raised by Tao and Watson (1987) regarding data fitting procedure. It is thus important to understand limitations of using polynomial fits if derivatives of the response function are desired.

Table 4 illustrates stability classifications at the same transition points as Table 1 but recalculated using curve fit-extrapolated air temperatures at 2.5 m. Although there were a few cases where stability classifications differed (ie. very stable vs. stable), in no case did the transition between stable and unstable/neutral conditions differ between the two situations. This indicates that temperature measurements obtained at the 4.6 and 9.8 m heights specified stability conditions accurately enough within one hour intervals.

TABLE 4. ATMOSPHERIC STABILITY RATIOS FOR FIVE SELECTED DATES USING AIR TEMPERATURE EXTRAPOLATED TO 2.5M AND TEMPERATURE MEASURED AT 9.8M IN THE STABILITY EQUATION.

Julian Day	Date	Time	Stability Classification	Stability Ratio	Wind Speed (m/s)	Air Temperature (C) extrapolated to 2.5m
106	15-Apr	0600	V-stable	4.90	1.23	9.04
		0700	V-stable	1.42	1.64	11.03
		0800	Neutral	0.00	2.73	13.70
		1700	Unstable	-1.70	0.23	24.22
		1800	V-stable	4.90	0.23	23.15
197	15-Jul	0600	V-stable	4.90	0.39	24.65
		0700	Unstable	-1.69	1.13	27.21
		1800	Unstable	-0.72	1.98	34.09
		1900	V-stable	4.90	0.67	31.30
229	16-Aug	0600	V-stable	4.90	0.23	14.72
		0700	Unstable	-1.70	0.23	17.18
		0800	Unstable	-1.70	1.22	22.56
		1800	Unstable	-0.71	2.26	29.20
		1900	V-stable	2.73	1.52	25.94
259	15-Sep	0700	V-stable	3.77	0.97	21.43
		0800	Unstable	-0.31	3.76	24.78
289	15-Oct	0700	Stable	1.05	1.93	7.67
		0800	Neutral	0.00	2.11	10.13
		1700	Unstable/neutral	-0.11	2.86	21.96
		1800	V-stable	1.79	3.76	19.35

Vertical Temperature Gradients and the Inversion Layer

Figures 8 through 12 illustrate vertical temperature gradients that indicate the presence of inversions. The 15 April plot (Figure 8) shows interesting differences between temperature trends at lower altitudes vs. higher altitudes. Very stable conditions still prevailed at 07:00 and figure 8 shows the inversion layer up to about 9.8 m above which neutral or unstable conditions appeared to exist. However spraying customarily occurs well below the 9.8 m altitude, so this finding would not be of practical benefit with regard to spraying (ie. spraying is still not warranted at 07:00). Likewise between 17:00 and 18:00, spraying should be stopped as the 18:00 curve also shows inversion to 9.8m but unstable conditions above that level. This is also consistent with very stable conditions at 18:00 as indicated in Figure 5.

Figure 9 illustrates the 15 July plot. By contrast with the 15 April plot, inversions are not indicated at 07:00 or 18:00, and the curves follow a consistent pattern as a function of altitude (except for an anomaly at 22.9m). The 16 August plot (Figure 10) shows a similar trend as the July plot, but an almost flat (but still negative) temperature difference with altitude. $[T_{Z_2} - T_{Z_1}]$ only equaled -0.02 C and $[T_{Z_2}$ - extrapolated $T_{Z_1}] = -0.04$ º C. Temperatures were very close to each other not indicating an inversion, and Table 4 indicates unstable conditions at 07:00 for 16 August. The behavior of Equation (1) can be illustrated with regard to wind speed. Wind was almost calm at 07:00 (0.23 ms-1) and then jumped to 1.22 ms-1 by 08:00. If wind speed is low but inversion conditions are not detected, then unstable conditions will prevail. Higher wind speeds imply more mixing, but the trend is towards neutral if

temperature differences are very small. Like the 15 April plot, the 16 September plot (Figure 11 (a)) indicated a temperature inversion and very stable conditions at 07:00. Air temperatures were much higher than in April, but a check of prevailing conditions (Weather Underground, 2016) indicated morning cloudiness until about 08:30. This would delay heating of the ground surface much as cooler air temperatures would. Wind speeds were high throughout the day and into the evening indicating neutral or unstable conditions into the evening (Figure 5; Table 4). The October plot (Figure 12 (a)) shows a similar inversion near the surface as in the April plot at 07:00; conditions were sunny and cool.

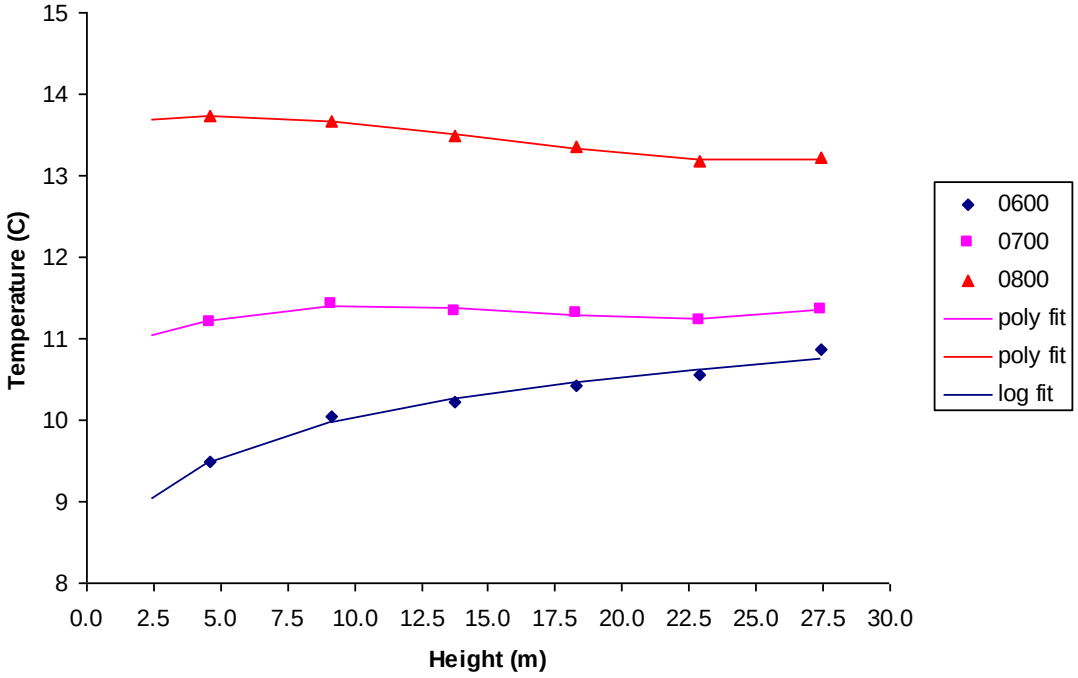

(a)

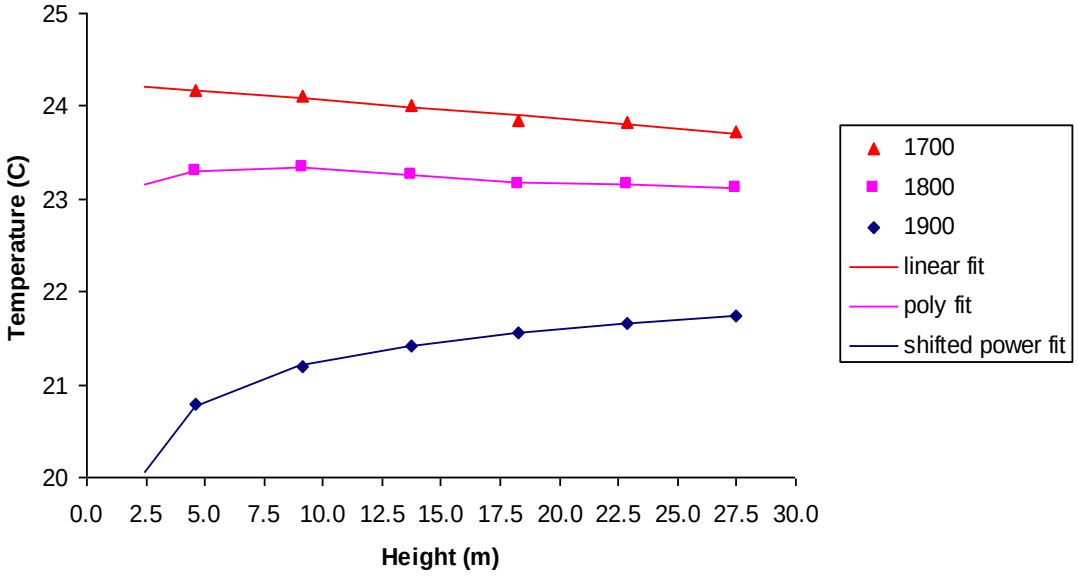

(b)

FIGURE 8. AIR TEMPERATURE AS A FUNCTION OF HEIGHT INDICATING MODEL EXTRAPOLATIONS FOR THE 2.5M HEIGHT OF TEMPERATURE ACQUISITION: (A) MORNING READINGS; (B) LATE AFTERNOON READINGS; 15 APRIL 2004).

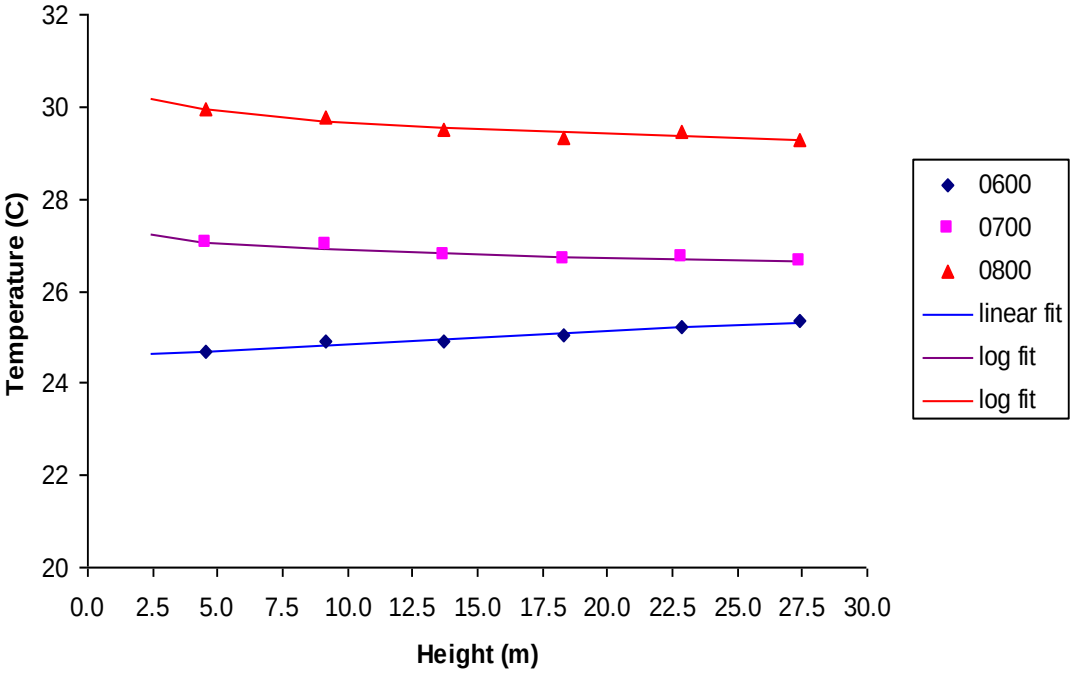

(a)

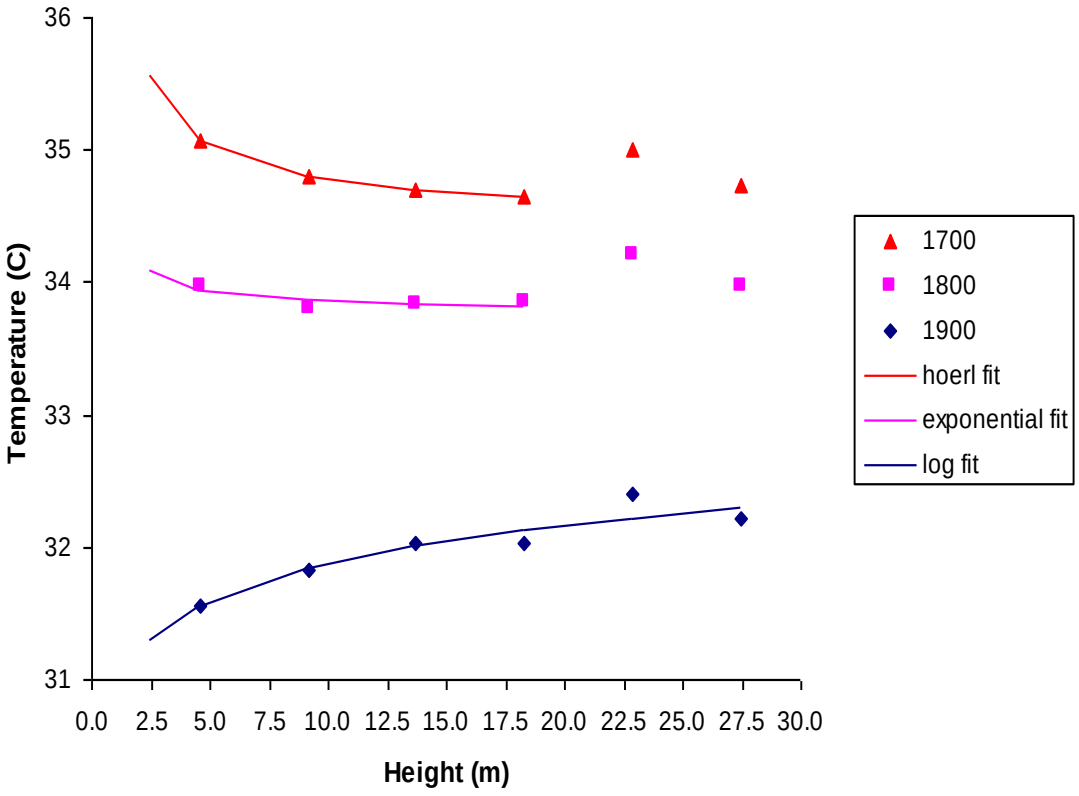

(b)

FIGURE 9. AIR TEMPERATURE AS A FUNCTION OF HEIGHT INDICATING MODEL EXTRAPOLATIONS FOR THE 2.5M HEIGHT OF TEMPERATURE ACQUISITION: (A) MORNING READINGS; (B) LATE AFTERNOON READINGS; 15 JULY 2004).

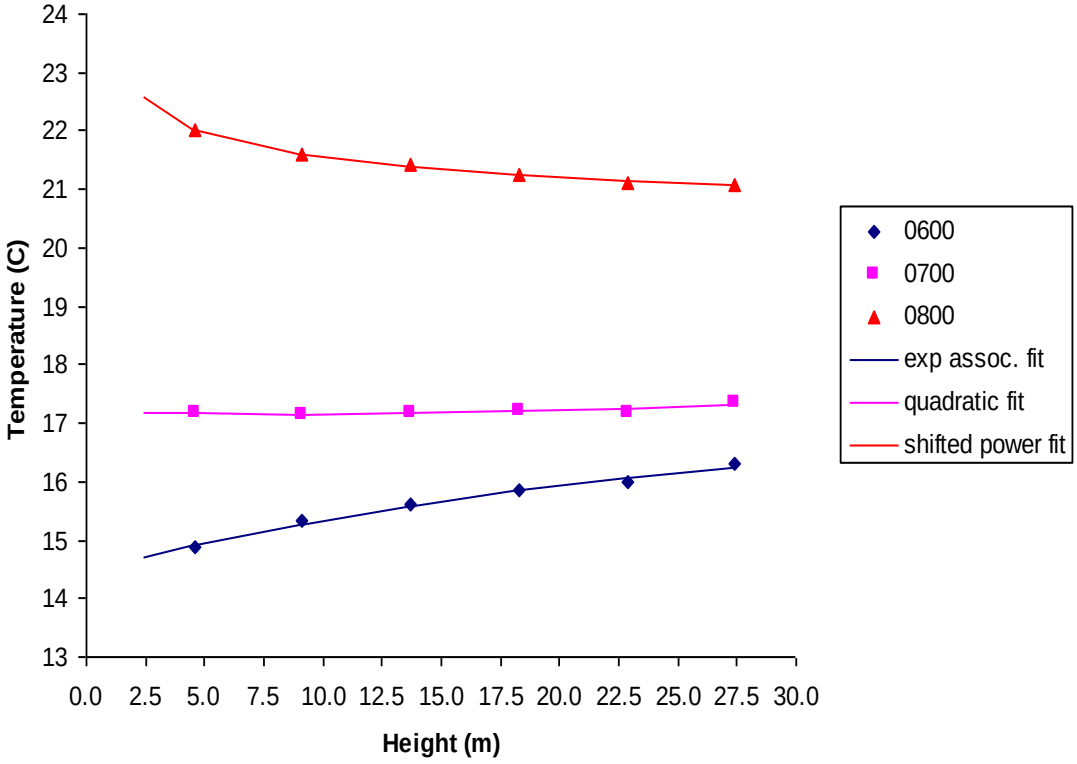

(a)

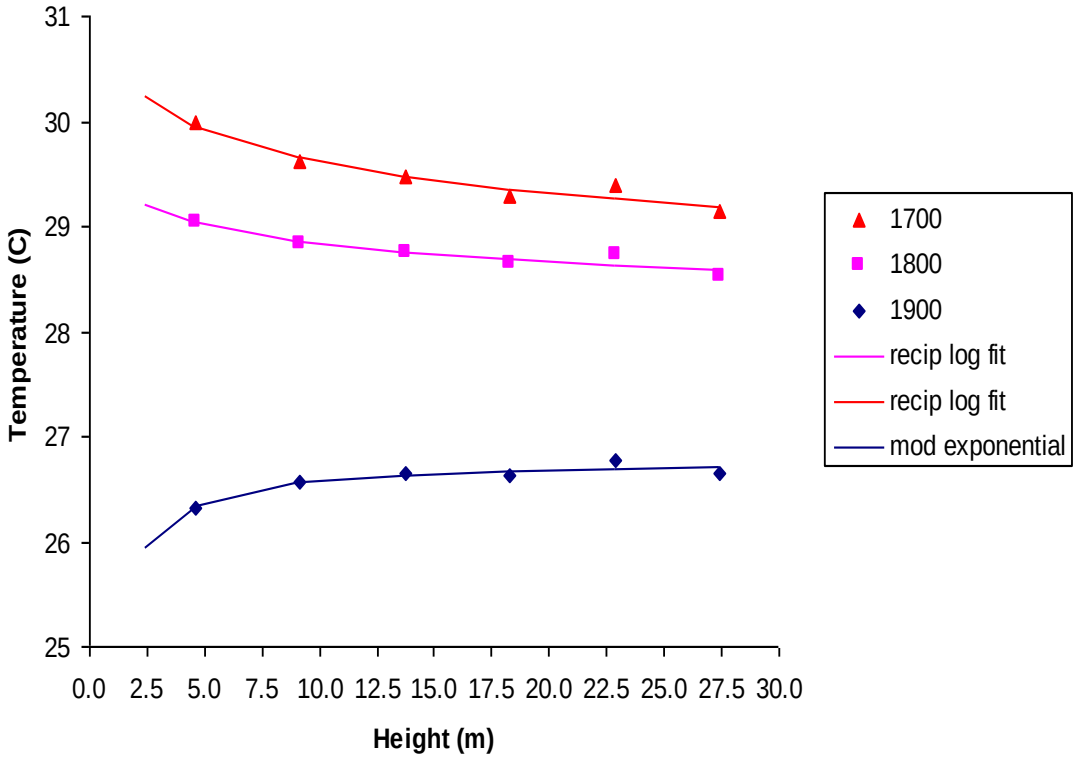

(b)

FIGURE 10. AIR TEMPERATURE AS A FUNCTION OF HEIGHT INDICATING MODEL EXTRAPOLATIONS FOR THE 2.5M HEIGHT OF TEMPERATURE ACQUISITION: (A) MORNING READINGS; (B) LATE AFTERNOON READINGS 16 AUG 2004).

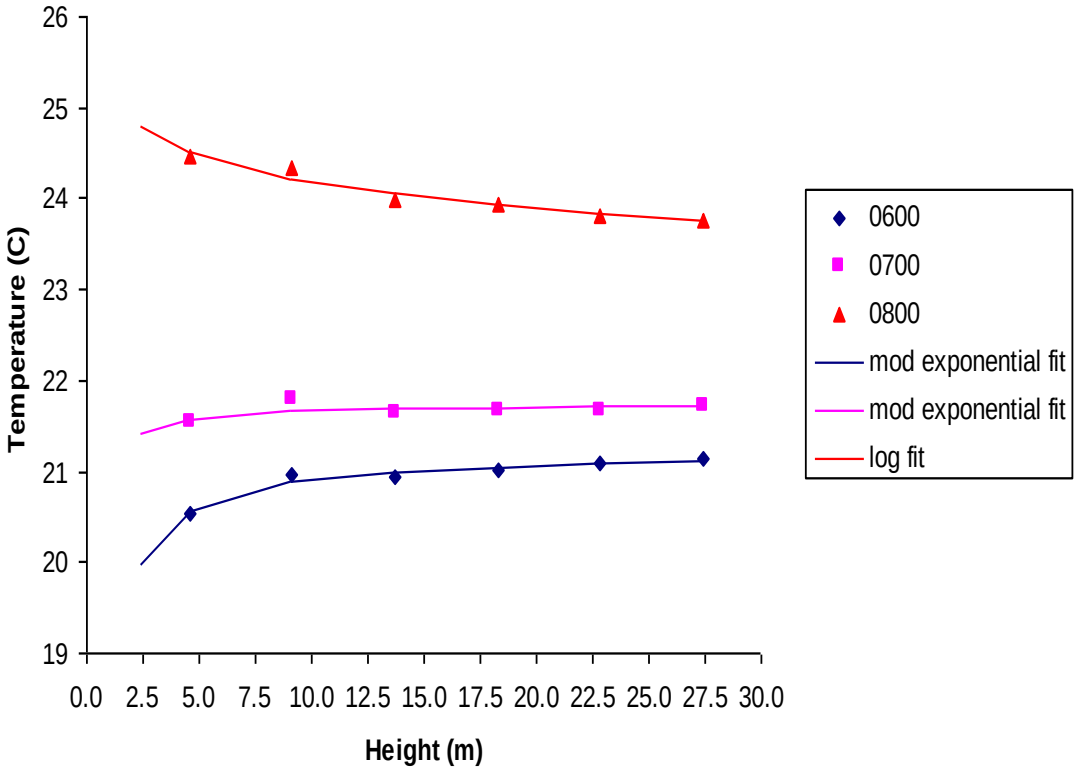

(a)

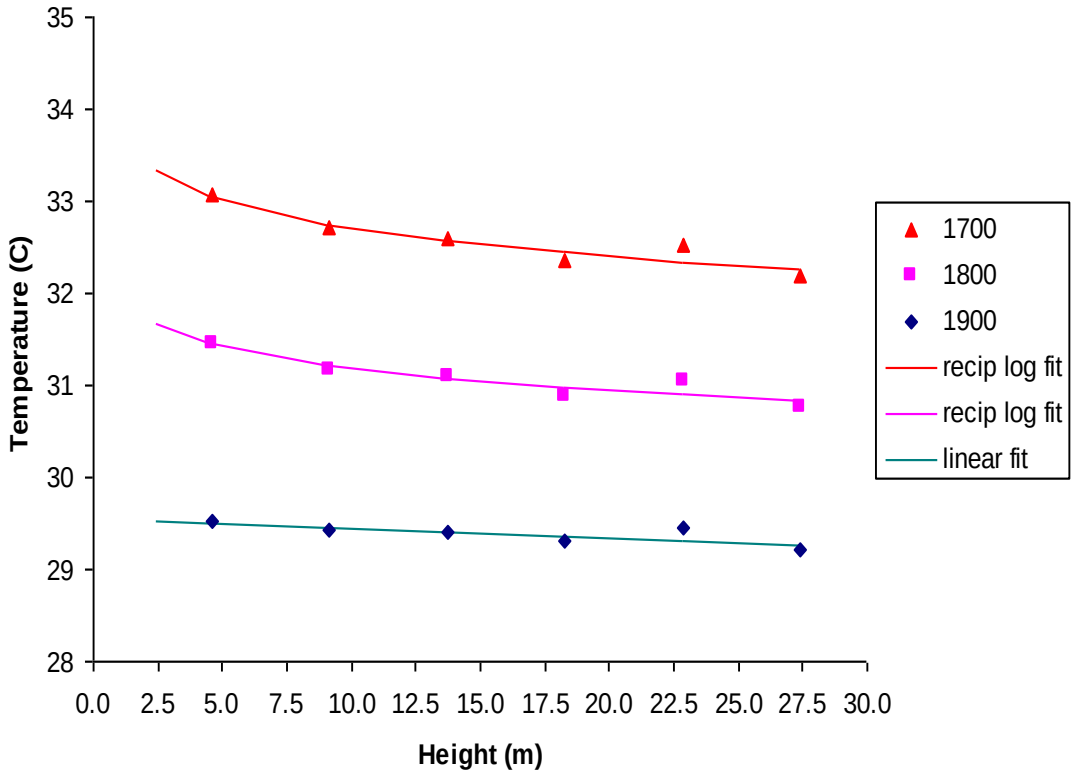

(b)

FIGURE 11. AIR TEMPERATURE AS A FUNCTION OF HEIGHT INDICATING MODEL EXTRAPOLATIONS FOR THE 2.5M HEIGHT OF TEMPERATURE ACQUISITION: (A) MORNING READINGS; (B) LATE AFTERNOON READINGS 15 SEP 2004).

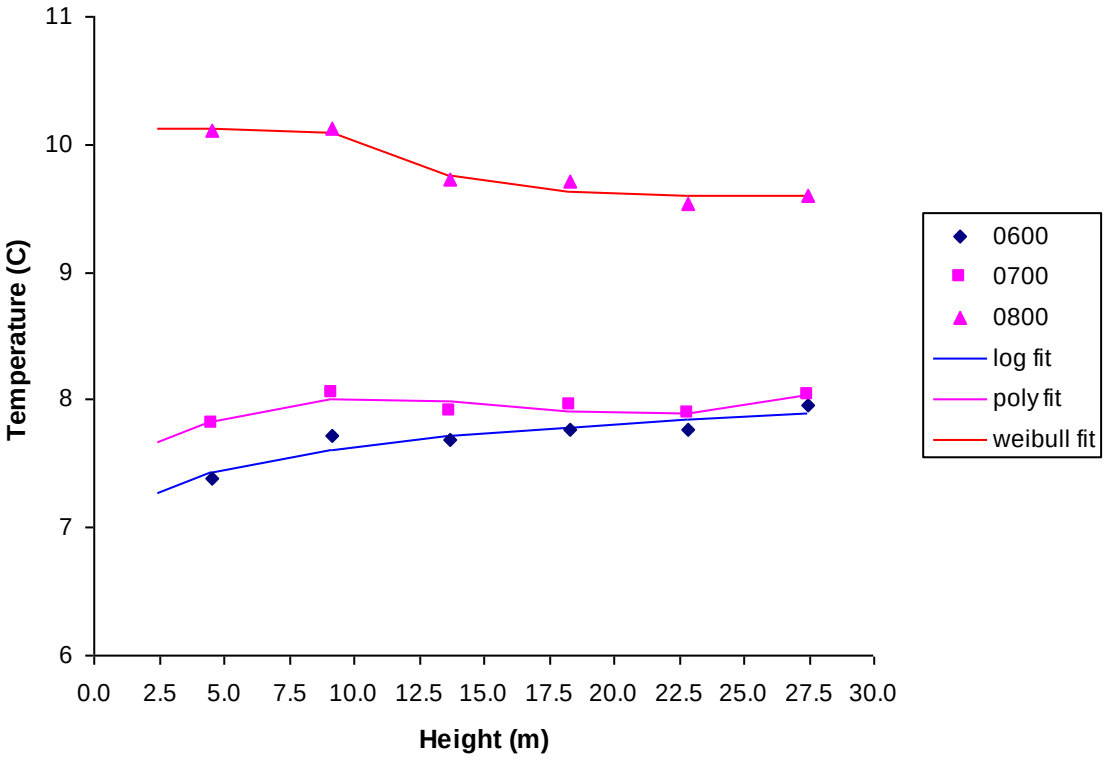

(a)

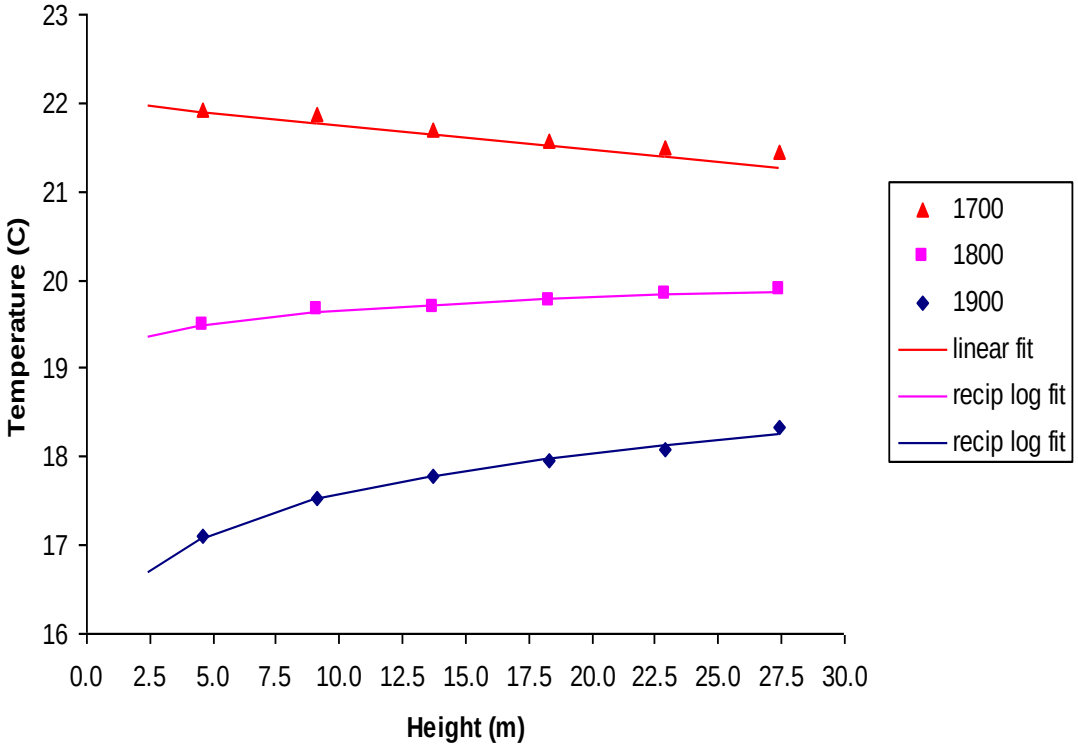

(b)

FIGURE 12. AIR TEMPERATURE AS A FUNCTION OF HEIGHT INDICATING MODEL EXTRAPOLATIONS FOR THE 2.5M HEIGHT OF TEMPERATURE ACQUISITION: (A) MORNING READINGS; (B) LATE AFTERNOON READINGS 15 OCT 2004).

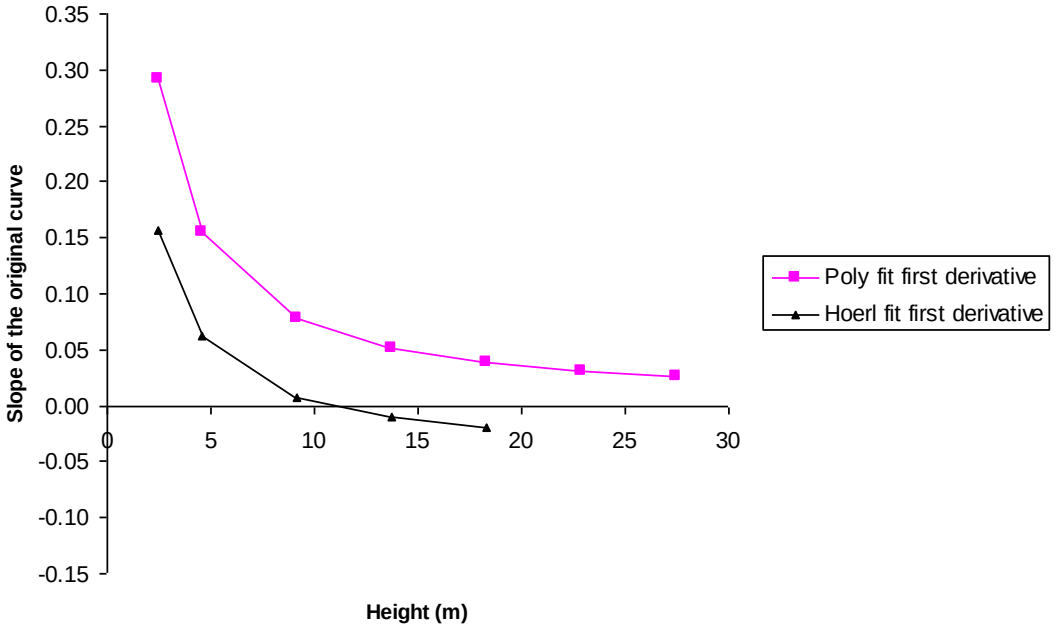

FIGURE 13. FIRST DERIVATIVE OF MODEL FITS TO AIR TEMPERATURE VS. HEIGHT DATA FOR 15 APRIL, 2004 ON FIGURE 8 (A).

Summary and Conclusions

Air temperature and wind speed data were taken at several heights to determine conditions necessary for stable atmosphere under which to avoid aerial spraying. These data confirm that solid recommendations can be made to pilots on times of day to watch for stable atmospheric conditions unfavorable for spraying. Cool or cloudy conditions delayed the time where spraying was permissable in the morning (to 0800 by our hourly analysis). An applicator should use judgment to find a balance between conditions that are so stable that spray does not disperse (with potential to move off-site), and conditions that are so unstable and windy that spray is quickly dispersed and moved off-site without reaching the target.

Results of this study suggest that guidelines on times of day and wind speeds below which spraying should be avoided can be identified. Results also evaluated guidelines developed for Arkansas that specify air temperature changes required during the morning and evening hours to avoid spraying under stable atmospheric conditions. When temperature criteria were satisfied, unstable conditions were achieved in all months indicated except for one month in the Spring. Stable atmospheric conditions persisted longer during the morning hours and began sooner in the evening under clear condiitons in cooler months of the scenarios indicated. It should be noted that during the daily cycle of atmospheric conditions, inversions occuring late in the afternoon are likely to persist through the remainder of the day. For a study such as this, high accuracy instrumentation was necessary to successfully determine temperature inversions, as vertical temperature gradients were very small in many cases.

Based on results, the following conclusions can be made:

- Temperature inversions were indicated before 07:00 and between 18:00 and 19:00 on days where ambient temperatures were high and conditions were clear.
- Cool or cloudy conditions delayed the time spray could take place safely by about one hour in the morning and moved back the time when spray should be halted by one hour in the late afternoon.
- Wind speed influenced the degree of atmospheric stability in concert with vertical temperature gradients. However, wind speed was not a good indicator of stable atmosphere by itself in narrow ranges of low to medium wind speed.
- Criteria for aerial applicators indicating stable, neutral, or unstable atmosphere were best indicated by

temperature differences with height. Recommendations made by the ASPB (2008) on temperature differences by which to gauge the likelihood of atmospheric stability were validated by our data at one hour intervals.

REFERENCES

[1] ASPB.Arkansas State Plant Board, Law and Regulations: Chapter 20-Arkansas Pesticide Use and Application Act and Regulations.Availableathttp://plantboard.arkansas.gov/Pesticides/Documents/ArkansasPesticideUseAndApplicationActAndRegulationsGreen(Rev %206-08).pdf, 2008. Accessed 17 October 2016.

[2] Bennett, D. 2, 4-D herbicide drift damage stuns east Arkansas cotton. Delta Farm Press. Aug 11, 2006. Available at: http://deltafarmpress.com/24-d-herbicide-drift-damage-stuns-east-arkansas-cotton, 2006. Accessed 17 October 2016.

[3] Beychok, M. R. 1994. Fundamentals of Stack Gas Dispersion. 3rd Ed., Newport Beach, CA: M.R. Beychock.

[4] Cooper, C.D., and Alley, F.C. 1994. Air Pollution Control: A Design Approach. 2nd Edition. Prospect Heights, Illinois: Waveland Press, Inc.

[5] CSIRO, 2002. Spray drift management. Collingwood, Victoria, Australia: CSIRO Publishing.

[6] FAO, Guidelines on Good Practice for Aerial Application of Pesticides. Food and Agriculture Organization of the United Nations, Rome, 2001. Available at http://www.fao.org/docrep/006/y2766e/y2766e00.htm, 2001. Accessed 17 October 2016.

[7] Fritz, B. L., W.C. Hoffmann, Y. Lan, S.J. Thomson, and Y. Huang. "Low-level atmospheric temperature inversions: characteristics and impacts on aerial applications", Agricultural Engineering International: the CIGR Ejournal. Manuscript PM 08 001. Vol. X., 2008.

[8] Lapworth, A. "The morning transition of the nocturnal boundary layer", Boundary-Layer Meteorology 119, 2006, pp. 501-526.

[9] Mahrt, L., J. Sun, W. Blumen, T. Delany, and S. Oncley. "Nocturnal boundary-layer regimes", Boundary-Layer Meteorology 88, 1998, pp. 255-278.

[10] MDAC. Rules of the Mississippi Department of Agriculture and Commerce. Available at http://sos.ms.gov/ACProposed/00016915b.pdf, 2016, Accessed 17 October, 2016.

[11] Miller, D.R. and T.E. Stoughton. "Response of spray drift from aerial applications at a forest edge to atmospheric stability", Agric. For. Meteorology 100, 2000, pp. 49-58.

[12] Munn, R.E. 1966. Descriptive Micrometeorology – Advances in Geophysics Supplement 1. New York: Academic Press.

[13] Ozkan, H.E. New nozzles for spray drift reduction. Ohio State University Extension Fact Sheet AEX-523-98. Available at http://ohioline.osu.edu/factsheet/fabe-523, 1998, Accessed 17 October 2016.

[14] Ramsey, G. Surface inversions, atmospheric stability, and spray drift. Pesticide Spray Drift Conference, Sacramento, California, Sept 5-6, 2002. Available at http://www.cdpr.ca.gov/docs/enforce/drftinit/confs/2001/ramsey.ppt, 2001, Accessed 17 October 2016.

[15] Stoughton, T.E., D.R. Miller, Y. Yang and K.M. Ducharme. "A comparison of spray drift predictions to Lidar data", Agric. For. Meteorology 88, 1997, pp. 15-26.

[16] Weather Underground. Weather history for 16 Sept 2004. Available at http://www.wunderground.com/history/airport/KGLH/2004/9/16/DailyHistory.html?req_city=NA&req_state=NA&req_statename=NA, 2011, Accessed 17 October 2016.

[17] Wiggins, S. EPA releases proposed pesticide applicator certification rule: Worker protection final rule expected this fall. Agricultural Aviation Sept/Oct, 2015, pp.14-15.

[18] Yates, W.E., N.B. Akesson, and R.E. Cowden. Criteria for minimizing drift residues on crops downwind from aerial applications. Transactions of the ASAE 17(4), 1974, pp. 637-632.

Inactivation Kinetics and Structural Changes of High Pressure Treated Actinidin

Pressure Effect on Actinidin Structure and Activity

Z.Alexandrakis[1a], G.Katsaros[*2a], Ph.Stavros[3b], G.Nounesis[4b], P. Taoukis[5a]

[a]Laboratory of Food Chemistry and Technology, School of Chemical Engineering, National Technical University of Athens, Zografou 15780, Greece

[b]Biomolecular Physics Laboratory, National Center for Scientific Research "Demokritos", 15310 Aghia Paraskevi, Greece

[1]zalexand@chemeng.ntua.gr; [*2]gkats@chemeng.ntua.gr; [3]third.author@first-third.edu; [3]third.author@first-third.edu; [5]taoukis@chemeng.ntua.gr

Abstract

Plant sulfydryl proteases such as actinidin are mainly used as meat tenderisers, milk clotting agents for the development of novel dairy products and proteolytic agents in biotechnological procedures. The main issue with regards their application is the method for the control of their enzymatic activity after the desired extent of proteolysis, considering that thermal treatment is not applicable. High Pressure (HP) processing could be applied for the enzyme activity regulation.

Actinidin, extracted from kiwi fruit (Hayward var., A. chinensis), was purified using anion-exchange and gel filtration chromatography. After purification procedure, only one single peak was finally received for this enzyme corresponding to a protein of molecular mass of 24 kDa with an isoelectric point equal to or lower than 3.5. The effect of HP (500–900MPa and 50-70°C) on the remaining activity of purified actinidin in phosphate buffer solution (pH 6.0) was studied. Inactivation of purified actinidin was described by a first-order kinetic model both for thermal and HP treatment at the studied processing conditions. Aiming at an optimal process design, a composite mathematical model, which describes the actinidin inactivation rate as a function of pressure and temperature conditions, taking into account the dependence of both activation energy and activation volume on the applied pressure and temperature respectively, was used.

HP-induced conformational changes of the purified actinidin were also investigated using Circular Dichroism spectroscopy (CD). A direct comparison of the CD results for the treated and the untreated enzymes reveals that reversible changes were depicted in the far- and near-UV. It is suggested that the exposure to HP may affect the linkage between thiolate ion of cysteine group and positively charged nitrogen of the imidazole group of the active site of actinidin leading to the reduction of the enzyme activity.

Keywords

Purified Actinidin; High Pressure Inactivation; Circular Dichroism; Structural Alterations

Introduction

Plant enzymes such as proteases are widely used in the food, pharmaceutical and detergent industries as well as in biotechnological applications. The most widely utilized plant proteases are the cysteine proteases (CPs) such as ficin (EC 3.4.22.3), papain (EC 3.4.22.2), actinidin (EC 3.4.22.14) and vromelain (EC 3.4.22.33) that may be extracted from Ficus carica, Carica papaya, Actinidia chinensis and Ananas comosus, respectively. The cysteine proteases (CPs) can be found in various parts of the plant, including fruits, stems, seeds and lattices (Boller, 1986) and take part in various cellular and extracellular processes such as fruit development and ripening (Brady, 1985), degradation of storage proteins in germinating seeds (Kembhavi *et al*., 1993; Taylor and Cuming, 1993), activation of pro-enzymes and degradation of defective proteins (Rudenskaya *et al*., 1998). The catalytic mechanism of these enzymes involves a cysteine and histidine group in the active site.

Actinidin has many similarities compared with the most studied enzyme of CPs, papain, with respect to the structure, the catalytic mechanism and the activation by reducing agents (Tello-Solis *et al*., 1995). On the other hand,

2327-7246/17/01 018-12 © 2017 DEStech Publications, Inc.
doi:10.12783/ijast.2017.0501.02

they differ in the amino acids lining, the substrate-binding pocket and in substrate specificity (Rawlings and Barrett, 1994 ; Gosalia *et al*., 2005). Actinidin consists of 220 amino acids with an apparent molecular weight of about 23.0 kDa (Kamphuis *et al*., 1985). Its complete amino acid sequence (Carne *et al*., 1978), the nucleotide sequence of the corresponding gene (Podivinsky *et al*., 1989), and the three dimensional structure (Varughese *et al*., 1992) have been determined.

Plant cysteine proteases can be used in food and beverage industry like meat tenderization (Sullivan and Calkins, 2010), removal of chill haze in beer, milk coagulation (Katsaros *et al*., 2010 ; Lo Piero *et al*., 2011), improvement in the processing quality of cereals and gelatin hydrolysis. In recent years, many researchers have reported that actinidin can aid processing, improve the product sensory charecteristics and increase the efficiency of operation in dairy industry. Recent studies conducted by Katsaros *et al*. (2010) suggested the application of either kiwi fruit powder rich in actinidin or kiwi juice in the production of dairy products as well as the use of high pressure as regulator of proteolytic activity of kiwi juice. Another study reported the use of actinidin as a potential alternative of natural calf rennet for the coagulation of milk leading to novel dairy products (Lo Piero *et al*., 2011). Puglisi *et al* (2011) concluded that the actinidin can be utilized as a preparatory treatment in the production of milk-based products characterized by a reduced content of undesirable proteins.

One of the major disadvantages for the industrial application of these enzymes in food industries is that they are extremely stable enzymes in terms of resistance to thermal, solvent and chaotropic denaturation. This provides difficulties in terms of developing an effective protocol to assure inactivation in the final product prior to consumption, avoiding excessive proteolysis. Technologies such as High Pressure (HP) processing that have potential to inactivate microorganisms (Hoover *et al*., 1989; Knorr, 1993) and enzymes (Katsaros *et al*., 2009a,b ; Alexandrakis *et al*., 2014), while providing advantages with regards sensory and nutritional quality, could be employed. However, the data on the inactivation kinetics using HP on proteases are limited (Katsaros *et al*., 2009a ; b). According to these studies, cysteine proteases (ficin, papain and crude actinidin) showed high thermal and pressure stability, requiring intense process conditions for adequate inactivation. Most of the studies on the inactivation by thermal and HP processing of crude or purified cysteine proteases do not investigate structural changes associated with the processing. The pressure-induced changes in the rate of enzyme-catalysed reactions may be attributed to changes in the structure of enzymes or/and changes in the reaction mechanism. In order to understand better the actinidin structure/function relationships, the mechanism of HP-induced inactivation of actinidin is worth investigating.

Circular dichroism (CD) is a technique used to give useful information about protein structure, the extent and rate of structural changes and ligand binding. CD is effective in investigating the conformational changes in proteins that occur as a result of changes in experimental parameters such as pH, pressure, temperature and binding of ligands. CD analysis has been the subject of many studies and gives important additional information about the effect of temperature (Balan *et al*., 2006 ; Thanassoulas *et al*., 2011), pH (Ramos, 2004; Ribeiro-Jr and Ramos, 2004), charge (Ramos *et al*., 1999; Regis *et al*., 2005), and ligands (Balan *et al*., 2006; Ramos *et al*., 2007) in the secondary and tertiary structure of proteins and enzymes (Menendez *et al*.,2006 ; Alexandrakis *et al*., 2014).

The main objective of the present research was to systematically study the effect of HP on the activity and structure of purified actinidin from kiwi fruit. Mathematical models have been used to describe pressure–temperature dependence of inactivation rate constants of enzymes (Stoforos *et al*., 2002; Polydera *et al*., 2004). Such models can be a useful tool in designing and optimizing HP processes.

Materials and Methods

Kiwi Fruit

Fresh ripe kiwi fruits (A. chinensis), Hayward var. grown in Pieria, Northern Greece were obtained directly by the Association Cooperatives of kiwi fruit producers. The kiwi fruits were peeled and pulped. The pulp was centrifuged at 10,000 g for 15 min. The supernatant was filtered and the clear juice (pH 3.9), that had a significant proteolytic activity due to the endogenous actinidin was used for the production of purified actinidin.

Extraction and Purification of Actinidin from Kiwi Fruit

The purified actinidin was produced from kiwi juice using the extraction procedure as described by Brocklehurst *et al*. (1981). Actinidin was extracted after a number of steps: centrifugation, ammonium sulphate fractionation (25-60%) and ultrafiltration. Fruit (1 kg) was blended in 0.5 L of extraction buffer (0.2 M L-cysteine solution buffer, pH 5.0, containing 0.8 mM Na2O5S2 and 1 mM EDTA), and the enzyme was extracted by stirring for 60 min. The mixture was centrifuged for 30 min at 10,000 g (4oC) and the enzyme was precipitated from the supernatant with ammonium sulphate up to 60% saturation during 48 h at 4°C. The precipitate was resuspended in 0.1 M potassium phosphate buffer, pH 6.0, and dialyzed for 48 h at 4 °C. After dialysis, the solution was stored at 0°C and used as crude extract for further purification. Actinidin was purified by a combination of anion exchange and gel filtration chromatography. The columns were attached to a FLPC (fast-protein liquid chromatography) system (Biorad, USA) and the eluate was spectrophotometrically measured at 280 nm. Chromatographic separation was performed at ambient temperature and the received fractions were stored at 4°C immediately after collection. A 20-mL volume of enzyme extract was loaded in an UNO Q (Biorad, USA) column (2.5x10cm), while continuously washed with 50 mM acetate buffer (pH 4.5) until total removal of unbounded proteins. Bounded proteins were eluted using NaCl in acetate buffer, of increased with time concentration, ranging from 0 to 0.5 M. The procedure was repeated at least 2 times for more efficient purification. On-line spectrophotometric analysis of the eluted fractions from major peak containing actinidin activity were pooled and concentrated at 4°C with Centricon microconcentrator (Amicon, 10-kDa cutoff membrane). Further separation of fractions was performed using gel filtration chromatography. Four (4) mL of partially purified actinidin (received after anion-exchange chromatography) was loaded into Sephacryl S-200 gel filtration column (GE Healthcare, USA). The column had previously been equilibrated in phosphate buffer solution (pH 6.0). The flow rate was 1.5 mL/min and fractions were collected every 5 minutes. IEF and SDS-PAGE electrophoresis were performed after chromatography separation in order to check the purity of obtained actinidin. All fractions were analyzed for actinidin activity and protein concentration. The protein concentration was determined spectrophotometrically according to Bradford (Bradford *et al*, 1976), while proteolytic activity was measured as described by Katsaros *et al* (2009b). The purified enzyme was used for thermal and HP experiments.

Due to proteolytic activity inhibition throughout the purification procedure, the purified enzyme was activated before treatments. Solutions containing 0.2 M phosphate buffer (pH 6.0, 25 μL), 0.1 M L-cysteine (100 μL), 0.1 M EDTA (10 μL) and deionised water (865 μL) thermally treated at 40°C for 10 min were used to activate the enzyme.

SDS-PAGE Electrophoresis

SDS/PAGE experiments were performed using a 4–20% Mini-PROTEAN TGX™ precast polyacrylamide gel (Biorad, USA) attached to a Mini-PROTEAN Tetra system (Biorad, USA). Samples were boiled for 5 min at 100 °C in a buffer containing SDS (2.5%) and β-mercaptoethanol (5%). Gel staining was performed with Coomassie brilliant blue staining. Unstained MW marker (Fermentas, USA) composed of native proteins with precise molecular weights (beta-galactosidase (116kDa), bovine serum albumin (66.2kDa), ovalbumin (45.0kDa), lactate dehydrogenase (35.0kDa), REase Bsp98I (25.0kDa), beta-lactoglobulin (18.4kDa) and lysozyme (14.4kDa)) was used.

IEF- PAGE Electrophoresis

IEF-PAGE (Isoelectric focusing-PAGE) experiments were performed using a polyacrylamide gel attached to a PhastSystem electrophoresis unit (Amersham Biosciences AB, Sweden). The pI standards used (pH 3.5-9.3) were obtained by GE Healthhcare company.

Enzyme Activity Assay

The hydrolytic activity of actinidin was determined using nitroanilidine-Z-N-BOC-L-lysine-4-nitrophenyl ester as a low molecular weight substrate (Katsaros *et al*., 2009b). The enzymatic activity was calculated from the initial rate of ester hydrolysis by determining nitroanilidine (NA) liberation within the given period of time. Hydrolysis of NA-Z-N-BOC-L-lysine-4-nitrophenyl ester was carried out in 100 mM phosphate buffer, pH 6.0 at 25°C. Reaction, after temperature equilibration, was initiated by the addition of 125 μl of kiwi juice or purified actinidin solution in a total volume of 2500 μl. The substrate concentration used was 0.8 mM ester. The NA liberation was monitored spectrophotometrically (Helios Spectrophotometer, Unicam, USA) at 348 nm and recorded every 30 s over 5 min.

Self hydrolysis of NA-Z-NBOC-L-lysine-4-nitrophenyl ester was determined by substituting the enzyme with buffer solution. The molar absorption coefficient of NA (E348nm = 5.68 x 104 M-1 cm-1) was used in the calculation. One unit (U) of activity was defined as the amount of the enzyme that liberates 1 μmol of NA per minute. All experiments were repeated at least three times.

Thermal Treatment

The effect of temperature treatment on the actinidin stability was examined. Aliquots in thin-walled glass test-tubes of 0.5 ml volume were placed in water-baths (WB/OB 7–45, MEMMERT GmbH + Co., KG, Schwabach, Germany) at temperatures in the range 40–72.5 °C for various periods of time. During thermal treatment temperature was monitored and recorded at 2 s intervals in a multichannel datalogger (CR10X, Campbell Scientific, Leicestershire, UK) by a type T thermocouple placed inside a capillary used as a temperature indicator.

High Pressure Treatment

Enzyme solutions were placed into 2 ml pouches (PP film) for HP experiments. HP inactivation experiments were conducted in triplicate at various combinations of pressure (200–900 MPa) and temperature (40–80°C) for appropriate processing times. The high pressure unit (Food Pressure Unit FPU 1.01, Resato International BV, Roden, Holland), comprised a pressure intensifier and a multivessel system consisting of six vessels of 45 mL capacity each, with a maximum operating pressure and temperature of 1000 MPa and 90°C. The pressure transmitting fluid used was polyglycol ISO viscosity class VG 15 (Resato International BV, Roden, Holland). Process temperature in the vessels was achieved by liquid circulation in the outer jacket controlled by a heating-cooling system. The desired value of pressure was set and after pressure build up (20 MPa/s), the pressure vessels were isolated. This point defined the time zero of this process. Pressure of each vessel was released after a preset time interval (according to the experimental design) by opening the pressure valve. The initial adiabatic temperature increase during pressure build up was taken into consideration in order to achieve the desired operating temperature during pressurization. Pressure and temperature were constantly monitored and recorded (in 1 s intervals) during the process.

Circular Dichroism Spectroscopy (CD)

Conformational changes leading to differences in the secondary and tertiary structure of actinidin were determined with a JASCO J-715 spectropolarimeter (Jasco, Easton, MD), equipped with a Jasco PTC 348 WI temperature controller. Wavelength scans in the far (200 to 260 nm) and the near (260 to 340 nm) UV regions were performed in Quartz SUPRASIL (HELLMA, Germany) precision cells of 0.1 cm and 1 cm path length, respectively. Each CD spectrum was obtained by averaging five to eight successive accumulation of data with a wavelength step of 0.2 nm at a rate of 50 nm min^{-1}, response time 2 s and a bandwidth of 2 nm. In all cases 0.15-0.4mg/ml protein concentration was used in 20mM phosphate buffer pH 6.0. Buffer spectra, obtained at identical conditions, have been subtracted from the raw data. The results in all experiments have been expressed as mean residue ellipticity in deg cm^2 / dmol. The CD spectra of all samples were measured immediately after thermal and high pressure treatment. The far and near UV spectra were analyzed by curve-fitting software ORIGIN 8.0 (OriginLab Corporation, USA) and for the calculation of secondary structural contents of the protein the CDNN software (Institut für Biotechnologie, Martin-Luther Universität Halle-Wittenberg) was used.

Kinetic Data Analysis

Values of enzyme activity (average of three different experiments) were plotted with time for different process conditions. The standard error between the three measurements is represented in the Tables with the ± standard deviation and in the figures with the error bars (each point in a figure represents one average value of three measurements). The technique of Model-based design of experiments was used for the experimental design in our study.

For statistical fit of the inactivation curves, least square regression analysis was conducted using SYSTAT 8.0 (SYSTAT 8.0 Statistics, 1998, SPSS Inc., Chicago, IL, USA) software. Dependence of inactivation rates on process parameters was described with appropriate mathematical equations, statistically treated by non-linear regression.

The high pressure and thermal stability of the enzyme is described by the parameters of the inactivation kinetics. Specifically, the inactivation of these enzymes can often be described by a first-order kinetic model (Eq.1):

$$\ln(\frac{A_t}{A_o}) = -k \cdot t \quad \text{(Eq.1)}$$

where Ao and At are the initial activity and the remaining activity at time t, respectively and k the inactivation rate constant (min-1). One-way ANOVA was applied to data and the differences between the means were tested by Duncan's test (P<0.05). Statistica 7.0 (Stat-Soft. Inc., USA) software was used for the statistical analysis.

The temperature dependence of the inactivation rate constant, k, as given by the Arrhenius relationship (Eq.2) was expressed in terms of activation energy, Eap.

$$k = k_{Tref} \cdot \exp\left[-\frac{E_{a_P}}{R} \cdot \left(\frac{1}{T} - \frac{1}{T_{ref}}\right)\right] \quad \text{(Eq.2)}$$

where T_{ref} is the reference temperature, k_{Tref} the inactivation rate (min^{-1}) at T_{ref} and R the universal gas constant (8.314 $Jmol^{-1}K^{-1}$).

Pressure effect on the reaction rate constant, k, was expressed through the activation volume, V_{aT} (mL/mol) and can be estimated by linear regression analysis using the Eyring equation :

$$k = k_{Pref} \cdot \exp\left[-\frac{V_{a_T}}{R} \cdot \frac{(P - P_{ref})}{T}\right] \quad \text{(Eq.3)}$$

where P_{ref} is the reference pressure, k_{Pref} the inactivation rate (min^{-1}) at P_{ref} and R the universal gas constant (8.314 $Jmol^{-1}K^{-1}$).

The effect of the applied pressure on the E_a values was described by an exponential equation (Eqn. 4), while the effect of process temperature on the V_a values was described by a linear equation (Eqn. 5) (Polydera *et al*., 2004).

$$E_a = E_{a_P} \cdot \exp[-b \cdot (P - P_{ref})] \quad \text{(Eq.4)}$$

$$V_a = a \cdot (T - T_{ref}) + V_{a_T} \quad \text{(Eq.5)}$$

Based on Eqns. 2 and 3 and taking into consideration of the effect of pressure on E_a values (Eqn. 4) and the effect of temperature on V_a values (Eqn.5), a multi-parameter equation was used to predict the inactivation rate constant at any combination of pressure and temperature conditions (Eq. 6).

$$k = k_{ref_{P,T}} \cdot \exp\left\{\begin{array}{l} -\frac{E_{a_P}}{R} \cdot \exp[-B \cdot (P - P_{ref})] \cdot \left(\frac{1}{T} - \frac{1}{T_{ref}}\right) \\ -\frac{A \cdot (T - T_{ref}) + V_{a_T}}{R} \cdot \frac{(P - P_{ref})}{T} \end{array}\right\} \quad \text{(Eq.6)}$$

Results and Discussion

Purification of Actinidin from Kiwi Fruit

Actinidin was purified from kiwi fruit. The steps of purification included precipitation with ammonium sulphate, anion exchange and gel filtration chromatography.

Actinidin bounded strongly to an anion-exchange column (UNOsphere Q) media at pH equal to 4.5, whereas most of the other proteins were eluted. Increasing the NaCl gradient, three peaks of different proteins were eluted. The actinidin was eluted at 0.17 M NaCl (Figure 1A). This sample was rechromatographed on anion-exchange column at pH=4.5 for further purification. Concentrated and pooled bounded actinidin containing fractions from anion exchange chromatography were next loaded onto the Sephacryl S-200 column. After gel filtration chromatography, only one single peak was finally received for actinidin at 215 min (Figure 1B). SDS-PAGE and IEF electrophoresis showed that the purified actinidin contained a single band of 24000 Da (Figure 2a) with an isoelectric point equal to or lower than 3.5 (Figure 2b). The purified enzyme showed specific activity 92.4 units/mg with approximately 12% recovery of the crude enzyme.

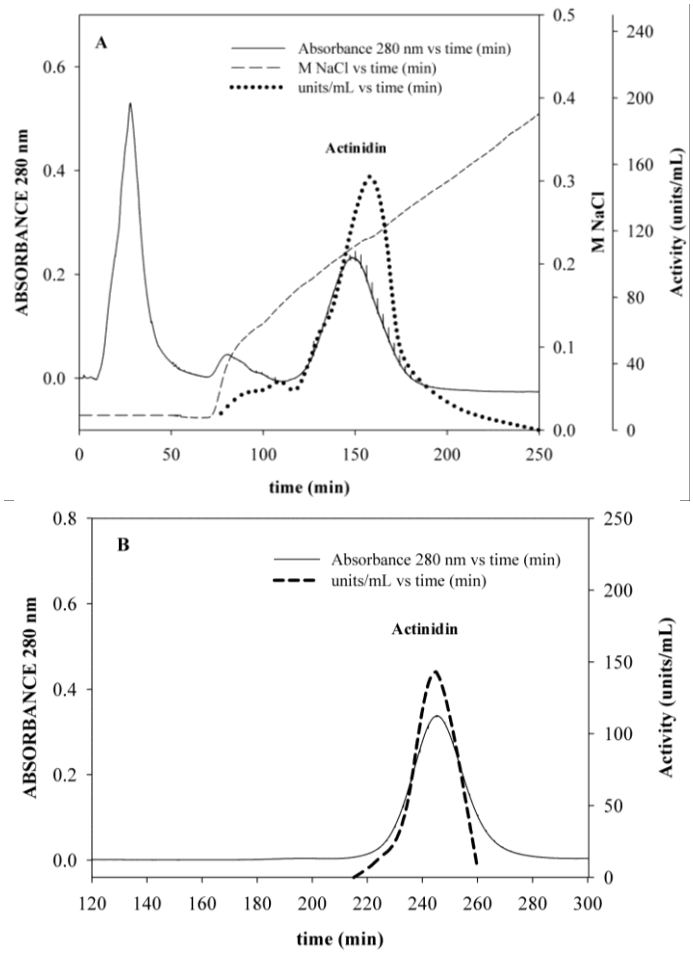

FIGURE 1. PANEL A. ELUTION PROFILE FOR THE ANION-EXCHANGE CHROMATOGRAPHY OF KIWIFRUIT ACTINIDIN ON UNOQ COLUMN. UNO Q WAS EQUILIBRATED IN 50mM ACETATE BUFFER SOLUTION (pH=4.5). PANEL B. ELUTION PROFILE FOR THE GEL FILTRATION CHROMATOGRAPHY OF KIWIFRUIT ACTINIDIN ON SEPHACRYL S-200 COLUMN. SEPHACRYL S-200 WAS EQUILIBRATED IN 50mM PHOSPHATE BUFFER SOLUTION (pH=6.0).

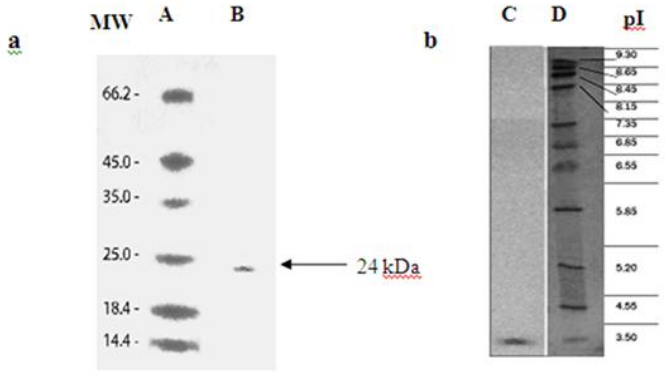

FIGURE 2. PANEL A. SDS-PAGE OF THE PURIFIED ACTINIDIN; LANE A, MW STANDARDS; LANE B, MW OF ACTINIDIN AFTER CHROMATOGRAPHY. PANEL B. IEF OF PURIFIED ACTINIDIN; LANE C, pI OF ACTINIDIN AFTER CHROMATOGRAPHY; LANE D, pI STANDARDS.

Thermal Inactivation

Data for isothermal inactivation of purified actinidin in phosphate buffer solution (pH 6.0) obtained in the temperature ranging from 60.0 to 72.5 °C could be accurately modeled applying the first-order kinetic model (Eq.1). No significant inactivation was observed for temperatures below 60°C for times up to 90 min. For purified actinidin from kiwi fruit, the inactivation rate constants (k, min^{-1}) obtained at each process temperature were estimated as 0.0077, 0.0096, 0.1567 and 0.4295 min^{-1} for processing at 65, 67.5,70 and 72.5°C, respectively. The values of k were calculated from non linear regression of Eq.1. The exponential fit is illustrated in Fig3. The square of the

correlation coefficient of the fit, R^2, was above 0.98 for all thermal experiments. The inactivation rate increased approximately 55-fold in the range of 65 to 72.5°C for purified actinidin. Compared these data with those obtained from Katsaros *et al*. (2009b), the actinidin in purified form is more resistant to temperature compared with the corresponding crude form. The inactivation of crude actinidin was achieved at lower temperatures (k 40°C = 0.0611 min^{-1}, k 45°C = 0.3776 min^{-1}, k 50°C = 1.6700 min^{-1}, k 55°C = 5.8951 min^{-1}). The temperature dependence of inactivation rate constants of purified actinidin in the temperature range studied was also investigated and expressed by the E_a value (175±23kJ/mol, R^2=0.989). This value is lower than that obtained by Katsaros *et al* (2009b) for this enzyme in crude form (267±42 kJ/mol, R^2=0.985).

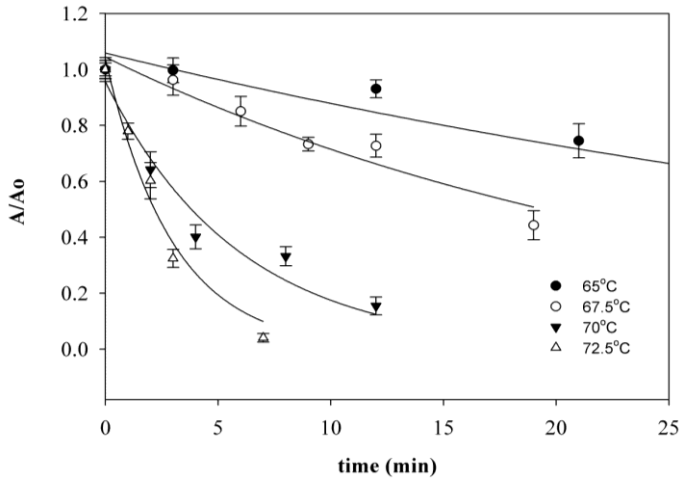

FIGURE 3. THERMAL INACTIVATION OF PURIFIED ACTINIDIN AT TEMPERATURES FROM 65 TO 72.5°C AT AMBIENT PRESSURE. PLOT OF % A/Ao VS. TIME; POINTS ARE EXPERIMENTAL MEASUREMENTS WITH STANDARD ERRORS AND SOLID LINES THE NON-LINEAR FIT OF EQ. (1).

Inactivation of Actinidin Subjected to High Pressure Treatment

Investigation of the effect of both pressure and temperature on the inactivation of proteolytic activity of purified actinidin was carried out. HP inactivation of studied enzyme was described by first-order kinetics (Eq.1), as in the case of thermal inactivation. The effect of temperature (50-70°C) and pressure (0.1-900 MPa) on proteolytic activity of purified actinidin is summarized in Table 1. Statistically significant differences ($p<0.05$) were observed between most of the k-values obtained for the inactivation of actinidin (Table 1), having as variables both temperatures (differences between temperatures at each pressure) or/and pressures (differences between pressures at each temperature). The increase of the applied high pressure (600 to 900 MPa) at each process temperature results in an increase of the inactivation rate constants (Figure 4). Up to 60°C purified actinidin inactivation rates in the pressure range studied are higher than the corresponding thermal rates at ambient pressure. In this range the high pressure effect is synergistic with temperature. However, at 70°C, thermal inactivation rate constants at all pressures studied are lower compared with the corresponding inactivation rate constants at ambient pressure and the same temperature. In this case the structural changes caused by the high pressure seem to act protectively (antagonistic effect).

TABLE 1. PURIFIED ACTINIDIN INACTIVATION RATE CONSTANTS (MIN^{-1}) AT DIFFERENT PRESSURE AND TEMPERATURE PROCESS CONDITIONS

T(C) P(MPa)	50	55	60	70	Ea (kJ/mol)
0.1	NE	NE	0.0363±0.0002^{1,a}	0.1567±0.0095^{2,a}	175.2±22.6^{a}
600	0.0084±0.0009^{1,a}	0.0113±0.0018^{2,a}	0.0128±0.0016^{2,b}	0.0274±0.0042^{3,b}	53.4±12.1^{b}
750	0.0115±0.0016^{1,b}	0.0159±0.0042^{1,a}	0.0247±0.0035^{2,c}	0.0398±0.0063^{3,c}	58.1±14.3^{b}
900	0.0206±0.0035^{1,c}	0.0284±0.0060^{1,b}	0.0374±0.0051^{1,a}	0.0661±0.0092^{2,d}	53.7±12.2^{b}
Va (ml/mol)	-7.98±2.59^{1}	-8.32±3.79^{1}	-9.89±2.51^{1}	-10.18±2.59^{1}	

Values of activation energy at constant pressures and values of activation volume at constant temperatures.
Average value ± standard error of regression. NE, not estimated.
Different superscript letters indicate significantly different means ($P<0.05$) within a column (differences between pressures)
Different superscript numbers indicate significantly different means ($P<0.05$) within a row (differences between temperatures)

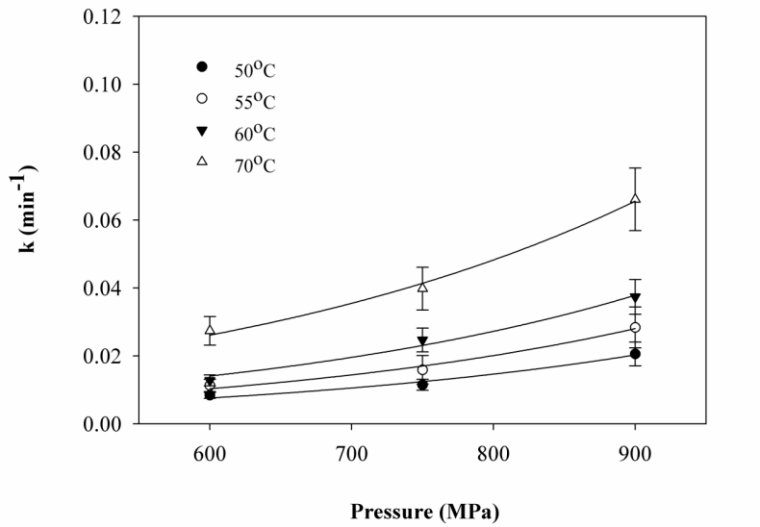

FIGURE 4. PURIFIED ACTINIDIN INACTIVATION RATE CONSTANTS AS A FUNCTION OF PRESSURE AND TEMPERATURE. POINTS ARE EXPERIMENTAL MEASUREMENTS WITH STANDARD ERRORS WITH STANDARD ERRORS AND SOLID LINES REPRESENT VALUES PREDICTED FROM EQ. (6).

The effect of temperature on the inactivation rate constants of studied enzyme was mathematically described by the Arrhenius equation. All the E_a values were estimated. The effect of pressure on the inactivation rate constants was described by the Eyring equation (Eq. 3). All the activation volume values, V_a, were also estimated for each studied temperature. Negative activation volumes indicate that pressure increase favors enzymes inactivation at a given temperature.

Based on Eqs. 2 and 3 and taking into consideration of the effect of pressure on E_a values (Eq. 4) and the effect of temperature on V_a values (Eq.5), the multi-parameter equation was used to predict the inactivation rate constant at any combination of pressure and temperature conditions (Eq.6). For purified actinidin, the parameters of the equation were estimated using non-linear regression routine (SYSTAT 8.0, Statistics 1998, SPCC Inc., Chicago, III, USA) (Table 2). The experimentally obtained k-values were very well correlated to the predicted values from the model. The same model has been used by Polydera *et al*. (2004) and Katsaros *et al*. (2009a,b), to describe pectinmethylesterase and proteases inactivation kinetics, respectively.

TABLE 2. PARAMETERS OF THE MULTI-PARAMETER EQUATION FOR PURIFIED ACTINIDIN INACTIVATION AT VARIOUS PRESSURE-TEMPERATURE CONDITIONS (P_{REF} = 600MPa, T_{REF}=323K).

PARAMETER	Estimated values (Purified actinidin)	95% confidence interval	
		Lower*	Upper*
$k_{ref\ P,T}$ (min^{-1})	0.007	0.006	0.009
E_{aP} (kJ/mol)	59.2	48.9	69.5
V_{aT} (ml/mol)	-9.0	-10.9	-7.1
B (MPa^{-1})	0.0012	0.0010	0.0023
A (ml/molK)	0.205	0.086	0.344
R^2	0.99		

*Upper and lower values were estimated for 95% confidence intervals by the non-linear regression routine (SYSTAT 8.0)

Compared these data with those cited in the literature for pressure inactivation of crude actinidin (Katsaros *et al*, 2009b), it was worth investigating the effect of different matrices on the stability of these enzymes against HP treatment. In Figure 5, the HP inactivation of actinidin (crude and purified forms) is presented. These enzymes were found to be more pressure sensitive in crude form compared to the purified form in a buffer system. Analyzing the results, it could be assumed that HP inactivation of purified enzymes was less pronounced than of crude enzymes meaning that the purified enzyme was more pressure stable. This conclusion could mean that pH or level of enzymes purification affects the degree of actinidin inactivation. The pH of buffer solution was close to 7 indicating that the enzyme pressure stability is increased at neutral pH values. Severe conditions based on combining high temperatures and high pressures were necessary to completely inactivate the purified enzymes.

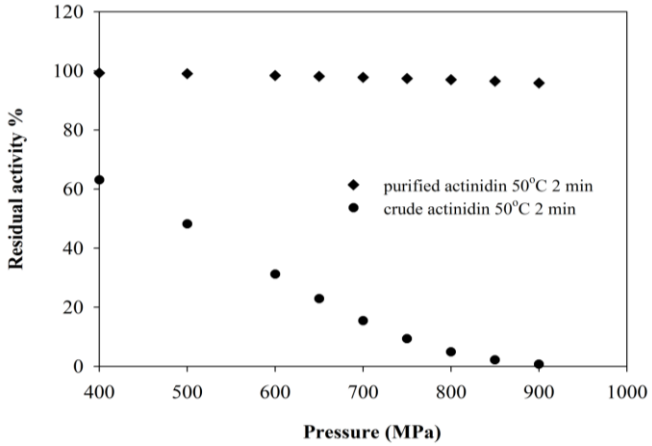

FIGURE 5. HIGH PRESSURE INACTIVATION OF PURIFIED AND CRUDE ACTINIDIN AT 50°C FOR 2 min.

Analysis of Actinidin Structure by Circular Dichroism Spectroscopy

High-pressure-induced structural changes upon the purified actinidin from kiwi juice were investigated using circular dichroism spectroscopy (CD). The experiments were carried out for temperatures around 60°C, well below the actinidin thermal denaturation limits. The CD spectra for the purified actinidin are presented in Figure 6. Spectra in the far-UV (wavelength region 190-260 nm) are presented in panel A and in the near-UV in panel B. The native actinidin exhibits one positive band at 190 nm and a negative extreme at 208 nm which is greater in magnitude than that at 220-222 nm. Similar secondary structure has been observed for proteinase Ω and papain (Solis-Mendiola, 1992). Analysis of the far-UV spectrum for the native molecule using CDNN software (Bohm *et al*., 1992) leads to 38.1 % helical content and 23.4 % beta sheets. These results are similar to what has already been published for the crystallogarphically solved structure of actinidin (Baker and Drenth, 1987).

In general, the pressure-induced conformational changes of an enzyme depend on its internal packing. The protein volume in solution contains voids and internal cavities, results of the imperfect packing of amino-acid residues as well as contributions due to solvation of peptide bonds and amino-acid side chains. For the actinidin, the HP induced spectra in the far-UV region presented in Fig. 6A reveal negligible differences with respect to the native, independently of the pressure level used for the treatment, i.e. for pressures 500, 750 and 900 MPa. This verifies that HP alone does not cause alterations upon the molecule's secondary structure. Pressure bears minimum effect upon the hydrogen bonds which are responsible for the secondary-structure network maintenance.

As in the case of the far-UV CD spectra, the near-UV CD spectra of the treated and untreated enzymes, associated to the molecule's tertiary structure (Woody, 1995), reveal reversible conformational changes (Figure 6B). Based on the three-dimensional structure of actinidin (PDB code 2ACT) (Picture 1), this molecule consists of a single chain of 220 residues, and is folded into two domains, domain I consisting of residues 19-115 and 214-218 and domain II residues 1-18 and 116-123 and contains three disulphide bridges (22-65, 56-98 and 156-206).

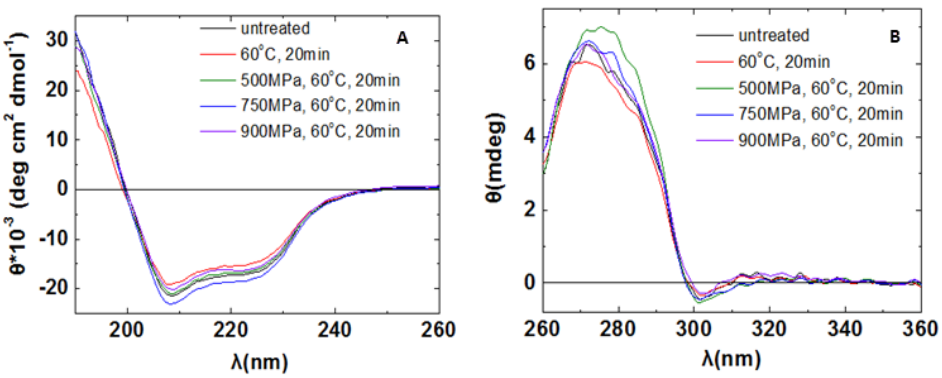

FIGURE 6. PANEL A, FAR-UV AND PANEL B, NEAR-UV CD SPECTRA FOR THE UNTREATED ACTINIDIN IN PHOSPHATE BUFFER (pH 6.0) AT 30°C (BLACK LINE); THERMALLY TREATED ACTINIDIN AT 60°C FOR 20 min (RED LINE), HIGH-PRESSURE-TREATED ACTINIDIN, AT 60°C AND 500 MPa FOR 20 min (GREEN LINE), AT 60°C AND 750 MPa FOR 20 min (BLUE LINE) AND AT 60°C AND 900 MPa FOR 20 min (PURPLE LINE).

Theoretical studies suggest that disulfide bonds stabilize proteins by reducing the entropy of the denatured state (Betz, 1993). Consequently, the tertiary structure of actinidin may remain fairly reversible even at 900 MPa due to a high number of disulfide bridges, which are known to stabilize its three dimensional structure.

As discussed previously, actinidin was progressively inactivated by increasing pressures. The residual activity obtained for the various processes were 45% for treatment at 900 MPa, 60 °C and 20 min, 62% for treatment at 750 MPa, 60 °C and 20 min and 80% for treatment at 500 MPa, 60 °C and 20 min. Taking into consideration of all the obtained results with regards the effect of pressure on the secondary and tertiary structure of actinidin, it may be assumed that the reduction of enzyme activity is not a result of the denaturation of major elements of the protein structure, but it may be correlated to the alteration of the precise spatial arrangement of residues in the active site. In the active enzyme, the thiolate (S~) ion (domain I) is believed to exist predominantly as an ion pair, with the positively charged nitrogen of the imadazole group (domain II) (Picture 1). It is suggested that HP may destabilize the hydrophobic aggregates, allowing water molecules to be forced into the enzyme interior. This will, in turn, affect the linkage between thiolate ion of cysteine group and positively charged nitrogen of the imidazole group of the active site of actinidin leading to the reduction of the enzyme activity.

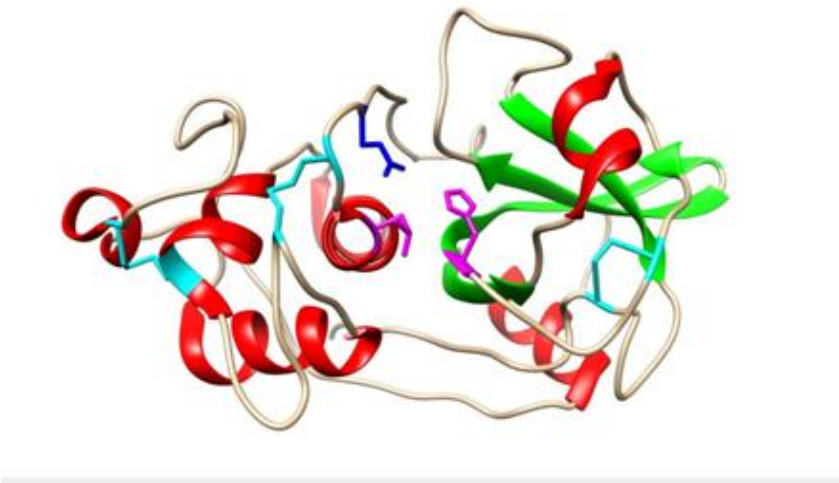

PICTURE 1. THE STRUCTURE OF ACTINIDIN (PDB CODE 2ACT). THE ACTINIDIN IS FOLDED INTO TWO DOMAINS, DOMAIN I (RESIDUES 19-115 AND 214-218) AND DOMAIN II (RESIDUES 1-18 AND 116-123) AND CONTAINS THREE DISULPHIDE BRIDGES (22-65, 56-98 AND 156-206) (LIGHT BLUE COLOUR). DOMAIN I CONSISTS MAINLY OF HELICAL SEGMENTS (RED COLOUR), WHILE DOMAIN TWO IS BUILT AROUND AN IRREGULAR TWISTED BETA SHEET (GREEN COLOUR). THE ARRANGEMENT OF CYS25 (PINK COLOUR, LEFT SIDE), WITH ITS FREE SULPHYDRYL GROUP, AND OF HIS162 (PINK COLOUR, RIGHT SIDE) ALONG WITH SOME OTHER RESIDUES IN CLOSE PROXIMITY ACT AS THE ACTIVE SITE OF THE MOLECULE.

Conclusions

Thermal and HP inactivation of purified actinidin was modeled by first order kinetics. The inactivation rate constants of the treated enzyme were expressed as a function of temperature and pressure enabling a proper design of high pressure treatments. A developed mathematical model, which describes the actinidin inactivation rate as a function of pressure and temperature conditions, taking into account of the dependence of both activation energy and activation volume on the applied pressure and temperature respectively, allows a better quantitative comparison of different treatments in the quest for an optimal process design. Purified actinidin appeared to be significantly resistant to pressure treatment. Severe conditions based on combining high temperatures and high pressures were necessary to inactivate this enzyme. Similar treatments reported previously in crude forms yielded higher enzyme inactivation rate, which implies that the matrix (composition and pH) play an important role in enzyme stability.

HP-induced structural changes upon the purified actinidin from kiwi juice have been investigated using circular dichroism spectroscopy (CD). Comparison of the CD spectra for the treated and the untreated enzymes reveals that HP does not cause alterations upon the molecule's secondary and tertiary structure (reversible conformational changes). HP may affect the arrangement of residues in the active site of actinidin leading to reduction of enzyme activity.

ACKNOWLEDGMENT

This research has been co-financed by the European Union (European Social Fund – ESF) and Greek national funds through the Operational Program "Education and Lifelong Learning" of the National Strategic Reference Framework (NSRF) - Research Funding Program: Heracleitus II. Investing in knowledge society through the European Social Fund.

REFERENCES

[1] Alexandrakis Z., Katsaros G., Stavros P., Katapodis P., Nounesis G. & Taoukis P.(2014). Comparative Structural Changes and Inactivation Kinetics of Pectin Methylesterases from Different Orange Cultivars Processed by High Pressure. Food and Bioprocess Technology. Volume 7, Issue 3, Pages 853-867.

[2] Balan A, Santa-Cruz CP, Moutran A, Ferreira RCC, Medrano FJ, Pérez CA, Ramos CHI & Ferreira LCS.(2006).The Molybdate-Binding Protein (ModA) of the Phytopathogen Xanthomonas axonopodis pv citri. Protein expression and purification, 50(2),215-222.

[3] Baker, E N, Drenth J.(1987). The thiol proteases: structure and mechanism. In Biological Macromolecules and Assemblies, eds Jurnak F A & McPherson A. John Wiley & Sons, New York, USA, pp 313-368.

[4] Betz S. (1993). Review:Disulfide bonds and the stability of globular proteins. Protein Science, 2, 1551-1558

[5] Böhm G, Muhr R & Jaenicke R .(1992). Quantitative analysis of protein far UV circular dichroism spectra by neural networks. Protein Engineering, 5(3),191-195.

[6] Boller T. (1986). Roles of proteolytic enzymes in interaction of plants with other organisms. In: Dalling MJ, editor. Plant proteolytic enzymes. Boca Raton, Florida: CRC Press; 1986.p. 67–96.

[7] Bradford, M. M. (1976). A rapid and sensitive method for quantitation of microgram quantities of protein utilizing the principle of protein-dye binding. Analytical Biochemistry, 72, 248-254.

[8] Brady CJ.(1985). Fruit ripening. Annu Rev Plant Physiol 38: 155-178.

[9] Carne A., Moore C.H., (1978). "The amino acid sequence of the tryptic peptides from actinidin, a proteolytic enzyme from the fruit of Actinidia chinensis", Biochem. J., vol. 173, p. 73-83.

[10] Galazka V B, Dickinson E, Ledward D A. (1996) Effect of high pressure on the emulsifying behaviour of b-lactoglobulin. Food Hydrocolloids 10, 213-219.

[11] Gosalia, D.N., Salisbury, C.M., Ellman, J.A., Scott, D.L. (2005). High throughput substrate specificity profiling of serine and cysteine proteases using solutionphase fluorogenic peptide microarrays. Molecular and Cellular Proteomics 4, 626–636.

[12] Hoover, D.G., Metrick, K., Papineau, A.M., Farkas, D.F., Knorr, D., (1989). Biological effects of high hydrostatic pressure on food microorganisms. Food Technology 43, 99–107.

[13] Kamphuis I.G., Drenth J., Baker E.N., (1985). "Thiol proteases: Comparative studies based on the high-resolution structures and on amino acid sequence information for Cathepsins B and H and stem bromelain", J. Mol. Biol., vol. 182, p. 317-329.

[14] Katsaros, G., Katapodis, P., Taoukis, P.S., (2009a). High hydrostatic pressure inactivation kinetics of the plant proteases ficin and papain. Journal of Food Engineering 91 (1), 42–48.

[15] Katsaros, G., Katapodis, P., Taoukis, P.S. (2009b). Modeling the effect of temperature and high hydrostatic pressure on the proteolytic activity of kiwi fruit juice. Journal of Food Engineering 94, 40–45

[16] Katsaros, G. I., Tavantzis, G., & Taoukis, P. S. (2010). Production of novel dairy products using actinidin and high pressure as enzyme activity regulator. Innovative Food Science and Emerging Technologies, 11, 47-51.

[17] Kembhavi AA, Buttle DJ, Knight CG, Barrett AJ.(1993). The two cysteine endopeptidases of legume seeds: purification and characterization by use of specific fluorometric assay. Arch Biochem Biophys 303: 208-213.

[18] Knorr, D. (1993). Effects of high hydrostatic pressure processes on food safety and quality. Food Technology 47, 156–161.

[19] Lo Piero, A.R., Puglisi, I., Petrone, G. (2011). Characterization of the purified actinidin as a plant coagulant of bovine milk. Eur. Food Res. Tech. 233, 517–524.

[20] Menéndez OH, Schwarzenbolz UR & Henle T. (2006). Structural changes of microbial transglutaminase during thermal and high-pressure treatment. Journal of Agricultural and Food Chemistry, 54(5), 1716-1721.

[21] Puglisi, I.; Petrone, G.; Lo Piero, A. R. (2011). Role of actinidin in the hydrolysis of the cream milk proteins. Food and Bioproducts Processing, 8-11.

[22] Podivinsky, E., Forster, R.L.S., Gardner, R.C. (1989). Nucleotide sequence of actinidin, a kiwi fruit protease. Nucleic Acids Research 17, 8363.

[23] Polydera, A.C., Galanou, E., Stoforos, N.G., Taoukis, P.S., (2004). Inactivation kinetics of pectin methylesterase of Greek Navel orange juice as a function of high hydrostatic pressure and temperature process conditions. Journal of Food Engineering 62, 291–298.

[24] Ramos CHI.(2004). A Spectroscopic-based Laboratory Course for Protein Conformational Studies. Biochemistry and Molecular Biology Education,32(1),31-34.

[25] Ramos CHI, Kay MS & Baldwin RL .(1999). Putative interhelix ion pairs involved in the stability of myoglobin. Biochemistry, 38(30), 9783-9790.

[26] Ramos CHI, Weisbuch S & Jamin M .(2007). Diffusive motions control the folding and unfolding kinetics of apomyoglobin pH 4 molten globule intermediate. Biochemistry, 46(14),4379-4389.

[27] Rawlings, N.D., Barrett, A.J. (1994). Families of Cysteine Peptidases. In: Barrett, A.J.(Ed.), Methods in Enzymology (Proteolytic Enzymes: Serine and Cysteine Peptidases), 244. Lavoisier, France, pp. 461–486.

[28] Regis WCB, Fattori J, Santoro MM, Jamin M & Ramos CHI. (2005). On the difference in stability between horse and sperm whale myoglobins. Archives of Biochemistry and Biophysics, 436(1),168-177.

[29] Ribeiro-Jr EA & Ramos CHI. (2004). Origin of the anomalous circular dichroism spectra of many apomyoglobin mutants. Analytical Biochemistry, 329(2),300-306.

[30] Rudenskaya GN, Bogacheva AM, Preusser A, Kuznetsova AV, Dunaevsky YE, Golovkin BN, *et al*. (1998). Taraxalisin – a serine protease from dandelion Taraxacum officinale Webb. S. I. FEBS Lett;437:237–40.

[31] Solis-Mendiola S., Arroyo-Reyna A. and Hernandez- Arana A. (1992). Circular dichroism of cysteine proteinases from papaya latex. Evidence of differences in the folding of their polypetide chains. Biochim. Biophys. Acta, I I I8 288-292.

[32] Stoforos, N.G., Crelier, S., Robert, M.C., Taoukis, P.S., (2002). Kinetics of tomato pectin methylesterase inactivation by temperature and high pressure. Journal of Food Science 67 (3), 1026–1031.

[33] Sullivan G.A., Calkins C.R.. (2010). Application of exogenous enzymes to beef muscle of high and low-connective tissue. Meat Science 85,730–734

[34] Taylor RM, Cumming AC. (1993). Purification of an endoproteinase that digests the wheat "EM" protein in vitro and determination of its cleavage sites. FEBS Lett 331: 76-80.

[35] Tello-Solis Salvador R., Valle-Guadarrama Maria Elena, Hernindez-Arana Andris, (1995). Purification and circular dichroism studies of multiple forms of actinidin from Actinidia chinensis (kiwifruit) Plant Science 106,227-232

[36] Thanassoulas A, Nomikos M, Theodoridou M, Stavros P, Mastellos D & Nounesis G (2011) Thermal and chemical denaturation of the BRCT functional module of human 53BP1. International journal of biological macromolecules, 49(3), 297-304.

[37] Varughese K.I., Cromwel. D., Hansain, S., Xuong, N., (1992) "Crystal structure of an actinidin-E-64 complex", Biochemistry, vol. 31, p. 5172-5176.

[38] Woody RW .(1995). Circular dichroism. Methods in Enzymology,246, 34-71.

Use of Unmanned Aerial Vehicles for Agricultural Applications with Emphasis on Crop Protection: Three Novel Case-studies

Panagiota Psirofonia[1],Vasileios Samaritakis[1], Panagiotis Eliopoulos[2], Ilyas Potamitis*[3]

[1]Dept. of Agriculture,Technological Educational Institute of Crete,PO BOX 1939 Postal Code 71004, Greece

[2]Technological Educational Institute of Thessaly,Department of Agricultural Technologists, Larissa 41110, Greece

[3]Dept. of Music Technology & Acoustics,Technological Educational Institute of Crete,E. Daskalaki Perivolia,74100, Rethymno Crete, Greece

*potamitis@staff.teicrete.gr

Abstract

The aim of this work is to introduce new applications for Unmanned Aerial Vehicles (UAVs) in Agriculture and especially in crop protection. All tests have been carried out in the island of Crete in Greece. Specific applications are: a) detection of symptoms (canopy discoloration) of pest or disease infestation on olive trees, b) mapping of Palm trees and identification of visible signs of infestation by the red palm weevil Rhynchophorus ferrugineus in large palm plantations, c) co-operation of UAV with electronic traps that automatically count insects and send counts to a server which, in turn summons and direct drones to spray in designated areas. Equipment and software, step by step methodology and practical applications of each of the three cases are described. We seek new application of drones in view to expand their possible uses that will allow them to penetrate the business of small to medium sized regional stakeholders. This work puts its emphasis on the practical details of the implementations, serving as a useful reference to relevant field-work.

Keywords

Unmanned Aerial Vehicle;Crop Protection;Olive;Palm Tree;E-trap

Introduction

UAVs are foreseen to become one of the technologies of the future. Satellites offer expensive services and do not satisfy the increasing need for spatial resolution and repeated controllable measurements for such application like monitoring of crop health and soil properties (e.g. plant growth, pest or disease development, irrigation problems etc.). UAVs have been proposed for repetitive tasks that are considered long and monotonous for humans or even dangerous [1,2].

In the context of precision agriculture applications UAVs appear in a broad spectrum of applications, including among many others: Assessment of water status and water stress effects in orchards [3], Chlorophyll content estimation [4], weed management [5], crop pest control [6], mapping of soil properties [7], estimating leaf carotenoid content in vineyards [8], development of spraying UAVs [9].

UAVs are routinely used as semi-automated crop scouting services in the sense that they are used to visually inspect fields but the images are interpreted by specialized users to improve management practices. Typical applications of UAVs include vegetation index maps that can be used for the analysis of agri-environmental measures [10-14].

However, technological advances penetrate slowly the routine practice of the majority of the cultivators as the latter rest unsure as to how this technology could lead to cost savings or revenue growth. To succeed in altering habits of decades we need to present case studies where technological advances meet the real needs of practitioners.

The broad objective of this research is to determine potential case studies of drones as a viable alternative for

2327-7246/17/01 030-10
doi:10.12783/ijast.2017.0501.03

manual crop scouting. It is an effort to expand possible utility so that agricultural unions and regional stakeholders can use the same technology in multiple applications under the same software umbrella. As the cost of image processing software to produce maps is big followed by the cost to purchase UAVs, one needs to identify an umbrella of practical, small scale applications that will allow this technology to penetrate small to medium size, regional stakeholders [1]. We put emphasis on practical issues and implementation details.

The specific aim of the present study is to evaluate the application of UAV in various crucial crop protection practices such as detection of pest symptoms on olive trees, identification of visible signs of infestation by the red palm weevil Rhynchophorus ferrugineus (Coleoptera: Curculionidae) in palm plantations and co-operation of UAV with electronic traps to achieve directed and targeted spraying of a designated area. The three cases (scenarios) are analytically presented below:

CASE A: Detection of Infestation Symptoms on Olive Trees

The cultivation of olive trees in Crete, occupies a very large part of the island's area. Approximately ¼ of the total area is covered by around 33 million olive trees, which constitute 65% of the agricultural land of the island [15]. The phytopathogenic bacterium Xylella fastidiosa, whose geographical distribution previously only included American countries and Taiwan, was recently encountered in Iran and in Europe as well. In particular, its first record in Europe referred in Southern Italy (Puglia region) in 2013 and concerns the detection and identification of a new and eminently destructive disease which affects the olive trees, commonly named "Olive Quick Decline Syndrome" (OQDS) [16]. Apparently, the inspection procedure for the early detection of the bacteria presence is extremely time consuming, taking into consideration the huge amount of olive trees in Crete (33 million trees) and in many other areas of Europe. Therefore it is necessary to find a detection process for all the olive trees in Crete with autopsy, which will be faster than the field inspection by experts, and immediately locate and remove all infected trees (eradication). The aim of this study is to get prepared for the strike of X. fastidiosa in Crete and to evaluate the use of the drone, for the identification of olive trees with dried foliage (yellowish discoloration in canopy), so that the olive trees that are suspected for infestation can be quickly located and then tested for the presence of X. fastidiosa, if it ever appears in the island of Crete.

CASE B: Mapping of Palm Trees and Detection of Rhynchophorus Ferrugineus Infestation Symptoms

The presence of the red palm weevil R. ferruginneus is confirmed by the official authorities in more than 30 countries in Asia and in the Mediterranean basin [17]. Wherever it has been located, its action has been devastating for the plantation of palms. Infested palm trees show a total loss of their leaves and rotting of the trunk which lead to the unavoidable death of the tree. Adult females lay eggs in the crown of palm trees, larvae then penetrate the crown and later to most parts of the upper trunk, forming tunnels of up to 1 m long. Many a time, the insect completes several generations inside the crown or trunk feeding on the inner tissues until the trunk or crown becomes hollow and tree gets killed. After the death of the palm adult weevils come out and seek fresh trees to attack [18]. The presence of R. ferruginneus has been verified in the island of Crete [19]. The cause of the high rate of spread of this pest is human intervention, by transporting infested young or adult date palm trees and offshoots from contaminated to uninfected areas. Date palm is an important crop in North African countries and ornamental palms are widely planted as amenity trees in the whole Mediterranean area. Three months after the infestation we have visible evidence of the palm decadence. As all palms are suitable for the development of the RPW there is a grave danger for the Cretan date palm Phoenix theophrastii that is found in the palm tree forest of Vai in Crete. Vai is the last palm tree forest on earth that is composed of this threatened plant species [20]. In case the pest is left undetected within a few weevil generations resulting in very severe overall damage. However, if detected on time, the damage can be minimized.

Hence the effort of using UAVs as a means of inspection is directed at early detection of infestation symptoms. The infested trees once located are destroyed and endangered trees are treated with insecticides. This treatment protects the rest of the trees from being infested.

CASE C: UAVs Co-Operating with E-Traps

We have developed e-traps adjusting our electronics in traps monitoring populations of pests in olive, cotton, grapes, fruits and apple cultivations, stored products, pines, and palm plantations [14-17]. In the present study, the possibility of a synergy between e-traps deployed in the field and UAVs used for targeted spraying is investigated. The application of pesticides is of crucial importance for crop protection. The use of UAVs is becoming increasingly common in carrying out this task mainly because of their speed, accuracy and effectiveness in the spraying operation [21, 22]. In our proof-of-concept scenario, an e-trap [23, 24, 25] calls a UAV (in practice this would be a spraying UAV), and submits its coordinates. The UAV accepts the call, flies to the given coordinates and performs a rectangular spraying flight having as its center the e-trap (i.e. simulating the spraying procedure) and returns to base.

Our findings are discussed on the basis of expanding UAV's possible uses in Agriculture, especially in crop protection, emphasizing on the practical details of the implementations.

Materials and Methods

Equipment and Software

We reference the equipment and software we used to capture image and video data to create geo-referenced maps and models.

UAVs Used

- DJI Phantom 3 Advanced UAV

The DJI Phantom 3 Advanced UAV was used to carry out the case-studies of this paper. The Phantom3-Advanced carries a fully stabilized 3-axis 1080p full HD video camera for smooth, videos and still photos. To allow you to see what the drone sees, DJI has engineered a new generation of their Lightbridge technology that allows 720p HD digital streaming of live video directly from the drone. You can control the camera and see video in real time as you fly and you can even share the video using the DJI Pilot app's advanced features. A wireless range of up to 3.1 miles line-of-sight is provided (depending on conditions).

Software Used to Control the UAV During the Flight

- DJI Go Android App (http://www.dji.com/product/goapp)

By using the DJI Go App the UAV operator can capture image and video data with the Phantom UAV and see exactly what the camera sees. It can track the aircraft's position and heading with a glance at a map.

- Pix4Dcapture (https://pix4d.com/product/pix4dcapture-app)

The Pix4D capture helps the UAV operator to select a flight plan and capture image data, ready for creating georeferenced maps and models in Pix4D or relevant photogrammetry desktop software.

Software Used to Post-Process the Images Taken from the UAV Flight

- MapsMadeEasy (https://www.mapsmadeeasy.com)

Maps Made Easy is a web application that lets users upload aerial photos, stitch the images and host created maps.

Software Used to Run the Simulation in UAV's Co-Operating with E-Traps Case Study

- Dronekit Python (http://python.dronekit.io/)

DroneKit-Python is an open source and community-driven project that allows developers to create apps that run on an on-board companion computer and communicate with the ArduPilot flight controller using a low-latency link. Onboard apps can significantly enhance the autopilot, adding greater intelligence to vehicle behaviour, and performing tasks that are computationally intensive or time-sensitive (for example, computer vision, path planning,

or 3D modelling). DroneKit-Python can also be used for ground station apps, communicating with vehicles over a higher latency RF-link. The API communicates with vehicles over MAVLink. It provides programmatic access to a connected vehicle's telemetry, state and parameter information, and enables both mission management and direct control over vehicle movement and operations. DroneKit-Python is compatible with vehicles that communicate using the MAVLink protocol (including most vehicles made by 3DR and other members of the DroneCode foundation). It runs on Linux, Mac OS X, or Windows.

- DronekitSitl (https://github.com/dronekit/dronekit-sitl)

The ArduPilot SITL (Software In The Loop) simulator allows you to simulate an ArduPilot based autopilot and communicate with it using MAVLink over the local IP network. DroneKit-SITL is a fast and easy way to run SITL on Windows, Linux, or MAC OSX. The tool is used extensively by DroneKit projects to test DroneKit apps and example code.

- MavProxy (https://github.com/ArduPilot/MAVProxy)

MavProxy is a UAV ground station software package for MAVLink based systems. MAVProxy is a fully-functioning GCS for UAV's. The intent is for a minimalist, portable and extendable GCS for any UAV supporting the MAVLink protocol (such as the APM).

UAV Application Procedure

Hereinafter, we describe the practical steps on how to use an UAV to capture image data, ready for creating geo-referenced maps and models based on available, state-of-the-art software. The following steps were followed in order to carry out the studies of this paper:

First, one needs to download and install a mission planning application that is compatible with the drone that is being used (e.g. Pix4Dcapture, Mission Planner, Drone deploy etc.). In this example the Pix4D capture application has been used to plan a mapping mission of a DJI Phantom 3 UAV.

Subsequently, the user through the software interface defines a single or multiple flight missions around the region of interest, taking account parameters like: altitude, drone speed, image overlap, camera angle, mission estimated time etc. for optimal results (see Fig. 1).

FIG.1 MISSION PLANNING APPLICATION EXAMPLE(PIX4DCAPTURE)

The user can define the region of interest by resizing, and panning the green window in the middle of the screen. The software application automatically calculates the region's area, the number of images needed, the spots where each image will be shot and the duration period of the mission. As a rule of thumb, it needs about 10 minutes to capture a 10 hectares region.

After the completion of the mission, depending on the user's needs, images can either be uploaded to a cloud service directly from the application and, therefore, the user receives a Quick 3D Preview, True Orthomosaic (Fig.

2), Digital Surface Model or NDVI vegetation index map among many other features. Alternatively, the user can just transfer the project directly from the drone to a computer and process it offline (e.g. locally by using Pix4dmapper, Agisoft Photoscan, OpenDroneMap etc. or on the cloud through the platforms of Maps made easy, Drone deploy etc.). In the following case studies the MapsMadeEasy online service was used, in order to create the true orthomosaic.

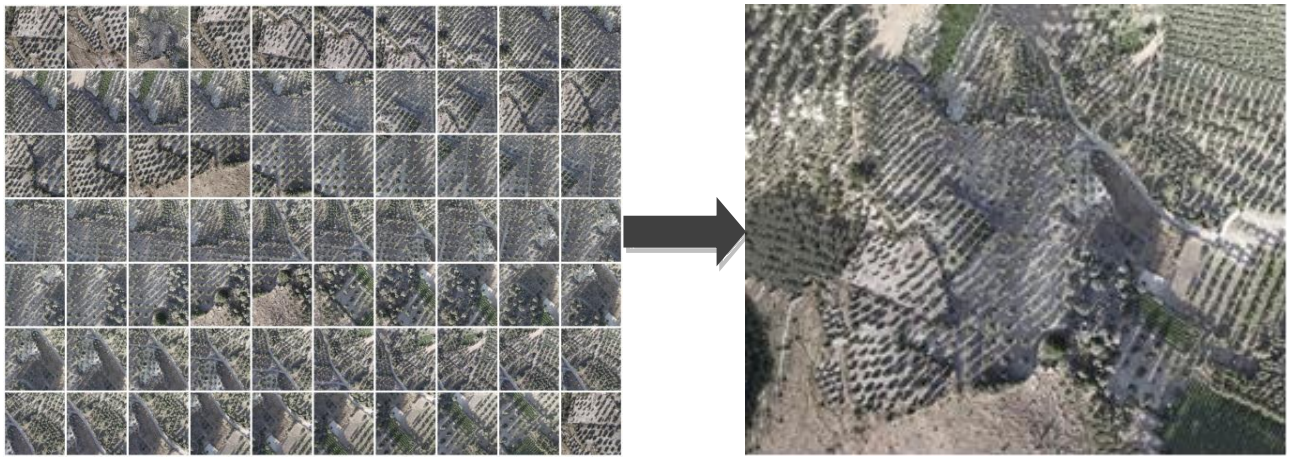

FIG.2 TRUE ORTHIMOSAIC-A SERIES OF OVERLAPPING AERIAL PHOTOGRAPHS TAKEN FROM THE UAV'S CAMERA(LEFT)THAT HAVE BEEN GEOMETRICALLY CORRECTED(ORTHORECTIFIED)(RIGHT)TO GIVE THEM A UNIFORM SCALE AND THEREFORE GIVES EXACT MEASUREMENTS AND CAN BE USED IN ANY GIS SOFTWARE.

Cooperation of UAV and E-Trap

For the purposed of the case 3 scenario, the e-traps carry SIM-cards and make use of the GPRS functionality to transmit counts of trapped insects to a server that keeps all information in a database. For handling the database and the information flow a Web Application is used, that is composed of two parts: a) The back-end, that runs on the Web Server is written in PHP and manages the database and b). TheFront End running in the web-browser, constitutes the user interface and is written in HTML5, CSS and JavaScript. The access to the database is through its Back End.We have implemented an application that sends an HTTP request and communicates with the Back End of the Web Application. The HTTP is a POST request, referencing a specific URL and has as ID the trap parameters. The back-end of the Web application includes PHP code to handle the request. The code reads the ID, and collects the relevant information from the database (i.e. counts, GPS coordinates). Then, it answers to the HTTP request with an HTTP response that returns the requested information in JSON form. The client-application that sends HTTP POST requests, is written in python using the library "requests". A second python script creates and uploads a mission to the UAV, where the UAV takes off, flies to the e-trap, performs a rectangular spraying flight of 25m2 having as its center the e-trap and returns to base. This drone action simulates the action of a spraying drone. The python script is executed on the base station when the number of insects recorded in the e-trap exceeds the predefined threshold. The server is the link between the e-traps and the UAV. It gathers the data from the e-traps and when the insects' number surpasses the threshold the script is executed.

Results and Discussion

CASE A: Detection of Infestation Symptoms on Olive Trees

We have examined the applicability of UAVs in identifying possible discoloration in the canopy of olive trees. The UAV's acquired images and video recordings were used to examine the olive grove for variations within crops. The variation within a single crop is caused by the natural variation in pheno- and genotype, as well as the individual history of the plant [14].

Olive trees with regional dried foliage were found in an olive grove in the area of Kato Asites in the district of Heraklion in Crete (35.18417° N, 24.99375° E).

In order to test the method, the UAV took a flight at a low altitude, in that specific olive grove, to scan the region. For this case a DJI Phantom 3 Advanced was used to visually check, in real time, for any abnormalities in the crown of the trees, by viewing the video feed on the screen of a tablet running the DJI GO application.

FIG.3 SCREENSHOTS OF THE VIDEO CAPTURED DURING THE FIRST PASS OF THE UAV FLIGHT SHOWING DISCOLORATIONS IN THE CROWN OF SOME OLIVE TREES

A discoloration of the crown of some trees was quickly noticed during this first pass and captured in video and images (Fig. 3). Emphasis was given to "suspicious" trees, by reducing the height of the flight. During this lower-altitude, second pass, the macroscopic inspection revealed peripheral drying at the bottom of the crown (Fig. 4).

FIG.4 SCREENSHOTS OF THE VIDEO CAPTURED DURING THE SECOND LOWER PASS OF THE UAV FLIGHT TEVEALING PERIPHERAL DRYING AT THE BOTTOM OG THE CROWN

Subsequently, the human operator of the drone defined a mission (Fig. 5) at a height of 50 meters to capture a series of 65 photos needed for the creation of a true orthomosaic (an image geometrically corrected which has a uniform scale and each pixel corresponds to a set of known coordinates and therefore gives exact measurements). The purpose of this action was to create point features with exact coordinates corresponding to each "suspected for infection" tree.

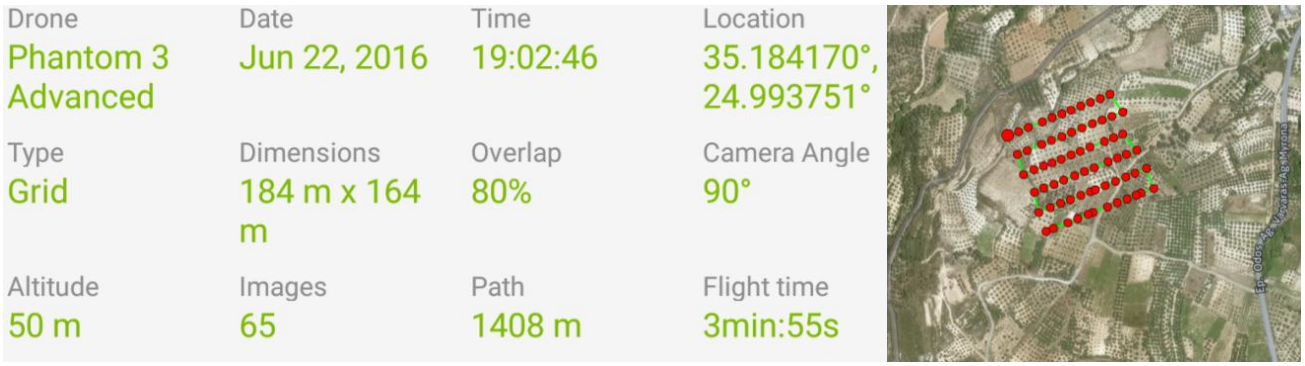

FIG.5 CHARACTERISTICS OF THE MISSION PLAN DEFINED TO CREATE A TRUE ORTHOMOSAIC IMAGE,ESSENTIAL FOR THE ACCRURATE POSITIONING OF THE INFECTED OLIVE TREES

By processing the data (high resolution geo-referenced image) it turned out that 26 olive trees had dried yellowish foliage in a single parcel (Fig. 6). The explanation for these symptoms was provided by the owner of the olive

grove, who explained that the dried foliage was due to a fire that could not be controlled. This theory was corroborated by the fact that damaged canopy parts were located at the lower branches of the trees.

FIG.6 HIGH RESOLUTION GEO-REFERENCED IMAGE(TRUE ORTHOMOSAIC)SHOWING THE 26 OLIVES TREES THAT HAD DRIED FOLIAGE

CASE B: Mapping of Palm Trees and Detection of Rhynchophorus Ferrugineus Infestation Symptoms

This section outlines how UAVs have been used in remote sensing for identifying visible signs of R. ferrugineus infestation in palms.

We investigate the applicability of drones to check-up quickly of a large number of palm trees with minor human intervention and a single case is described below. A drone was flown as close as 1 to 5 meters from a palm tree plantation in Afrathias, Tympaki (35.0458^{o} N, 24.76038^{o} E). For this case a DJI Phantom 3 Advanced was used to detect any abnormality in the crown of the palm trees, by viewing in real time the video feed on the screen of a tablet running the DJI GO application. Emphasis was given to the palm trees that appear to have abnormalities in their crown. Still images and video were captured during the flight to be analysed afterwards(Fig. 7). After the analysis the palm trees were divided into 3 categories and marked with different colours (Fig. 8): dead palm trees (marked in yellow), ostensibly healthy palm trees (marked in green) and palm trees with visible signs of infestation (marked in red).

FIG.7 DETAIL ON A PALM PLANTATION(35.04625^{o} N, 24.75948^{o} E)SHOWING VISIBLE SIGNS OF INFESTATION ON THE LEAVES, DEMONSTRATING THE POSSIBLE USE OF UAVS IN GPS TAGGING AND SURVEILLANCE OF PALM PLANTATIONS

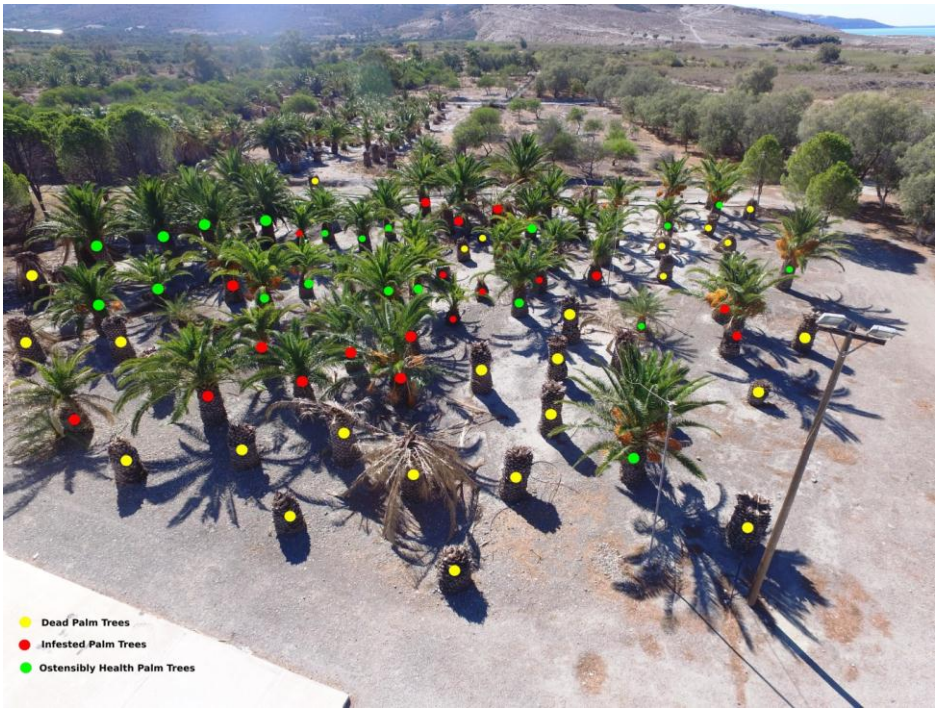

FIG.8 PALM PALM PLANTATION(35.04625° N, 24.75948° E)INSPECTED WITH AN UAV.DEAD PALM TREES(MARKED IN YELLOW),OSTENSIBLY HEALTHY PALM TREES(MARKED IN GREEN)AND PALM TREES WITH VISIBLE SIGNS OF INFESTATION(MARKED IN RED)

CASE C: UAVs Co-Operating with E-Traps

Before testing the script on a real UAV a simulation was run using the tools of Drone Kit, Drone Kit-Sitl and MavProxy. The scenario was that our base station (lat: 35.317844°, lon: 25.103059°) gets a signal that an e-trap located 250m to the east (lat: 35.317844°, lon: 25.105493°) exceeds the predefined threshold of the 30 insects. The base station server subsequently initiates the mission and an UAV is sent to the e-trap, performs the rectangular flight and after 2 minutes returns to the base and lands. The whole procedure is described in Fig. 9.

We foresee that the successful execution of this scenario has the potential of revolutionizing the treatment of large plantations. Networks of electronic monitoring traps sample pest's populations, send their accumulated data wirelessly through the GSM network to a central monitoring station. The central agency automatically decides when and where to send spraying drones and is guided by the traps to spray from low-altitude and effect surgical hits.

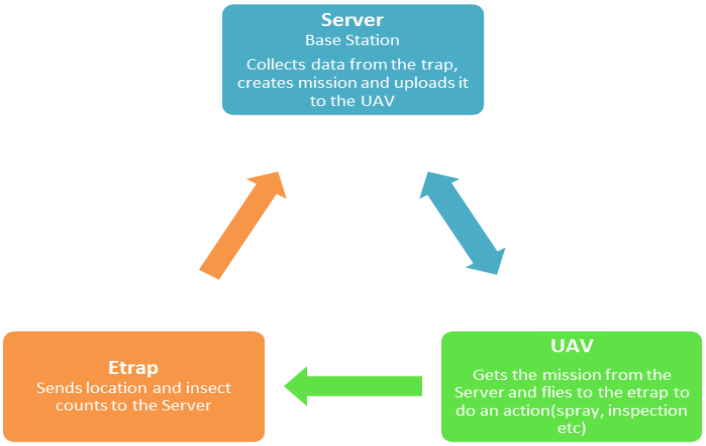

FIG.9 DIAGRAM SHOWING HOW AN E-TRAP LOCATED ON A TREE SENDS DATA TO THE BASE SERVER,WHICH CONSEQUENTLY SETS AN UNMANNED AERIAL VEHICLE IN MOTION,MISSIONED TO FLY TO THE E-TRAP,SPRAY THE TREE IF NEEDED AND RETURN TO THE BASE.

Conclusion

UAVs appear with a main role in an increasing number of applications in agricultural and environmental tasks. Their use and future prospect is constantly celebrated. However, their use penetrates slowly the routine practice of the majority of the cultivators as the latter rest unsure as to how this technology could eventually lead to cost savings or revenue growth. This paper is augmenting the number of possible uses of this technology with new applications that have been carried out in the island of Crete in Greece. Our aim is to introduce this technology to small/medium regional stakeholders in an effort to help them face their crop protection problems related to the effectiveness of common detection methods and to reduce their monitoring costs. Moreover, by increasing the number of possible tasks carried out by the same stakeholder by re-using the same technology it is possible to improve the cost to benefit ratio for acquiring this technology and offering a sustainable, high-technology service to the community.

REFERENCES

[1] Zhang, C., and Kovacs, J.M. "The application of small unmanned aerial systems for precision agriculture: a review", Precision Agriculture, Vol. 13.6, pp. 693-712, 2012.

[2] Matese, A., Toscano, P., Di Gennaro, S.F., Genesio, L., Vaccari, F.P., Primicerio, J., Belli, C., Zaldei, A., Bianconi, R. and Gioli, B. "Intercomparison of UAV, Aircraft and Satellite Remote Sensing Platforms for Precision Viticulture", Remote Sens., Vol. 7, pp. 2971-2990, 2015.

[3] González-Dugo, V., Zarco-Tejada, P.J., Nicolás, E., Nortes, P.A., Alarcón, J.J., Intrigliolo, D.S. and Fereres, E. "Using high resolution UAV thermal imagery to assess the variability in the water status of five fruit tree species within a commercial orchard", Precision Agriculture, Springer Science, doi: 10.1007/s11119-013-9322-9, 2013.

[4] Kempeneers, P., Zarco-Tejada, P.J., North, P.R.J., De Backer, S., Delalieux, S., Sepulcre-Cantó, G., Morales, F., Van Aardt, J.A.N., Sagardoy, R., Coppin, P. and Scheunders, P. "Model inversion for chlorophyll estimation in open canopies from hyperspectral imagery", International Journal of Remote Sensing, Vol. 29, Iss. 17-18, pp. 5093-5111, 2008.

[5] Torres-Sánchez, J., López-Granados, F., De Castro, A.I. and Peña-Barragán, J.M. "Configuration and Specifications of an Unmanned Aerial Vehicle (UAV) for Early Site Specific Weed Management", PLoS ONE 8(3): e58210. doi:10.1371/journal.pone.0058210, 2013.

[6] Lelong, C.C.D., Burger, P., Jubelin, G., Roux, B., Labbé, S. et al. "Assessment of unmanned aerial vehicles imagery for quantitative monitoring of wheat crop in small plots", Sensors, Vol. 8, pp. 3557–3585, doi: 10.3390/s8053557, 2008.

[7] López-Granados, F., Jurado-Expósito, M., Peña-Barragán, J.M. and García-Torres, L. "Using geostatistical and remote sensing approaches for mapping soil properties", European Journal of Agronomy, doi: 10.1016/j.eja.2004.12.003, Vol. 23, No. 3, pp. 279-289, 2005.

[8] Zarco-Tejada, P.J., Guillén-Climent, M.L., Hernández-Clemente, R., Catalina, A., González, M.R. and Martín, P. "Estimating leaf carotenoid content in vineyards using high resolution hyperspectral imagery acquired from an unmanned aerial vehicle (UAV)", Agricultural and Forest Meteorology, ISSN 0168-1923, http://dx.doi.org/10.1016/j.agrformet.2012.12.013, Vol. 171–172, pp. 281-294, 2013.

[9] Giles, D.K. and Billing, R. "Unmanned aerial platforms for spraying: deployment and performance". Aspects of Applied Biology, No. 122, pp.63-69, 2014.

[10] Berri, O. and Peled, A. "Spectral indices for precise agriculture monitoring", International Journal of Remote Sensing, Vol 27, pp. 2039-2047, 2006.

[11] Jensen, T., Apan, A., Young, F., Zeller, L. and Cleminson, K. "Detecting the attributes of a wheat crop using digital imagery acquired from a low-altitude platform", Computers and Electronics in Agriculture, Vol. 59, pp. 66–77, 2007.

[12] Hunt, E.R., Hively, W.D., Fujikawa, S.J., Linden, D.S., Daughtry, C.S.T. and McCarty, G.W., "Acquisition of NIR green-blue digital photographs from unmanned aircraft for crop monitoring", Remote Sensing, Vol. 2, pp. 290–305, 2010.

[13] Leon, C. T., Shaw, D. R., Cox, M. S., Abshire, M. J., Ward, B., Wardlaw, M. C. and Watson, C. "Utility of remote sensing in predicting crop and soil characteristics", Precision Agriculture, Vol. 4, pp. 359–384, 2003

[14] Berni, J., Zarco-Tejada, P. J., Suarez, L., and Fereres, E. "Thermal and narrowband multispectral remote sensing for vegetation monitoring from an unmanned aerial vehicle", IEEE Transactions on Geoscience and Remote Sensing, Vol. 47, pp. 722–738, 2009.

[15] Hellenic Statistical Authority, 2013 ANNUAL AGRICULTURAL STATISTICAL SURVEY, http://www.statistics.gr, 15pp, 2016.

[16] EPPO, PM 7/24 (2) : "Xylella fastidiosa". Bulletin OEPP/EPPO Bulletin, 0 (0), 1–38 (in press), http://onlinelibrary.wiley.com/doi/10.1111/epp.12327/epdf, 2016.

[17] Giblin-Davis, R.M., Faleiro, J.R., Jacas, J.A., Peña, J.E., and Vidyasagar, P.S.P.V. "Coleoptera: Biology and management of the red palm weevil, Rhynchophorus ferrugineus", In J. E. Peña [ed.], Potential Invasive Pests of Agricultural Crop Species. CABI. Wallingford, UK, pp. 1–34, 2013.

[18] El-Mergawy, R.A.A.M. and Al-Ajlan, A.M., "Red palm weevil, Rhynchophorus ferrugineus (Olivier): economic importance, biology, biogeography, and integrated pest management", J. Agric. Sci. Technol. A1, 1e23, 2011.

[19] Kontodimas, D. C., Milonas, P. G., Vassiliou, V., Thymakis, N., and Economou, D. "The occurrence of Rhynchophorus ferrugineus in Greece and Cyprus and the risk against the native Greek palm tree Phoenix theophrasti". Entomol. Hellenica Vol. 16, pp.11–15, 2006.

[20] Johnson, D. "Phoenix theophrasti. The IUCN Red List of Threatened Species" e.T38630A10140653,http://dx.doi.org/10.2305/IUCN.UK.1998.RLTS.T38630A10140653.en, 1998.

[21] Faical, B.S., Costa, F.G., Pessin, G., Ueyama, J., Vieira, H.F., Colombo, A., Fini, P. H., Villas, L., Osorio, F. S., Vargas, P. A. and Braun, T. "The use of unmanned aerial vehicles and wireless sensor networks for spraying pesticides", Journal of Systems Architecture, Vol. 60, Iss. 4, pp. 393-404, 2014.

[22] Costa, F., Ueyama, J., Braun, T., Pessin, G., Osorio, F. and Vargas, P. "The use of unmanned aerial vehicles and wireless sensor network in agricultural applications", Geoscience and Remote Sensing Symposium (IGARSS), 2012 IEEE International, pp. 5045–5048, 2012.

[23] Potamitis, I. and Rigakis, I., "Insect surveillance at a global scale and the Internet of Things". EcoSummit Ecological Sustainability: Engineering Change, Montpellier, France, 2016.

[24] Potamitis, I., Rigakis, I. and Fysarakis, K. "Insect Biometrics: Optoacoustic Signal Processing and Its Applications to Remote Monitoring of McPhail Type Traps", PLoS ONE 10(11): e0140474, doi: 10.1371/journal.pone.0140474, 2015.

[25] Potamitis, I., Rigakis, I. "Smart traps for automatic remote monitoring of Rhynchophorus ferrugineus (Coleoptera: Curculionidae)", Peerj Preprints, 2015.